Progressive orocline formation in the Eastern Pontides–Lesser Caucasus

MAUD J. M. MEIJERS[1,2]*, BRIGITTE SMITH[3], DANIEL PASTOR-GALÁN[4],
RENZO DEGENAAR[4], NINO SADRADZE[5], SHOTA ADAMIA[6], LILIT SAHAKYAN[7],
ARA AVAGYAN[7], MARC SOSSON[1], YANN ROLLAND[1], COR G. LANGEREIS[4] &
CARLA MÜLLER[8]

[1]*Université de Nice Sophia-Antipolis, Observatoire de la Côte d'Azur, Géoazur UMR7329,
Faculté des Sciences, bat. 1 250 rue Albert Einstein, Sophia-Antipolis, 06560 Valbonne, France*

[2]*Department of Earth Sciences, University of Minnesota, 291 Shepherd Laboratories,
100 Union Street SE, Minneapolis, MN 55455, USA*

[3]*Université de Montpellier, INSU-CNRS, Laboratoire Géosciences Montpellier,
Place E. Bataillon, 34095 Montpellier Cedex 5, France*

[4]*Utrecht University, Paleomagnetic Laboratory Fort Hoofddijk, Faculty of Geosciences,
Budapestlaan 17, 3584CD Utrecht, the Netherlands*

[5]*Department of Mineral Resources, LEPL Alexandre Janelidze Institute of Geology,
Geochemistry and Isotope Geochronology, 30, T. Tabidze Street, 0179 Tbilisi, Georgia*

[6]*Javakhishvili Tbilisi State University, Institute of Geophysics, 1 M. Alexidze Street,
0193 Tbilisi, Georgia*

[7]*Institute of Geological Sciences, National Academy of Sciences of Armenia,
24a Baghramian Avenue, Yerevan 0019, Armenia*

[8]*PL 66-431 Santok, Ludzislawice, Poland*

Corresponding author (email: meijersmaud@gmail.com)
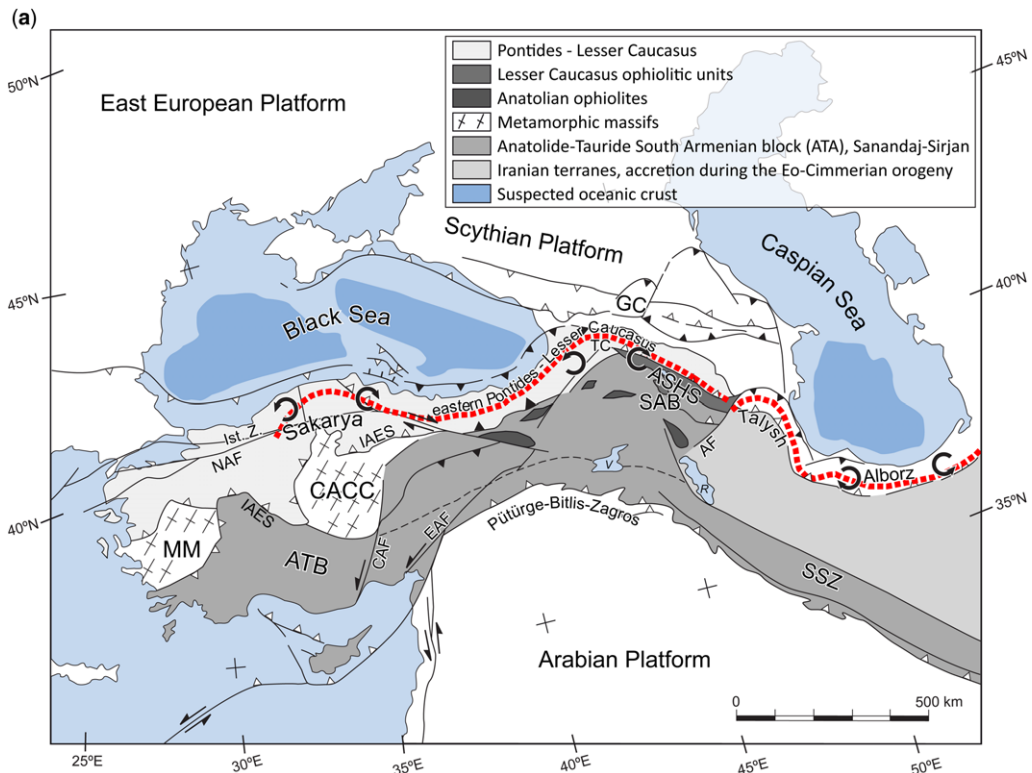
Abstract: The Eastern Pontides–Lesser Caucasus fold–thrust belt displays a peculiar northwards arc-shaped geometry that was defined as an orocline in earlier studies. The Lesser Caucasus was affected by two main tectonic events that could have caused orocline formation: (1) Paleocene–Eocene collision of the South Armenian Block with Eurasia; and (2) Oligocene–Miocene Arabia–Eurasia collision. We tested the hypothesis that the Lesser Caucasus is an orocline and aimed to time the formation of this orocline. To determine the vertical axis rotations, 37 sites were sampled for palaeomagnetism in rocks of Upper Cretaceous–Miocene age in Georgia and Armenia. In addition, we compiled a review of c. 100 available datasets. A strike test was applied to the remaining datasets, which were divided into four chronological sub-sets, leading us to conclude that the Eastern Pontides–Lesser Caucasus fold–thrust belt forms a progressive orocline. We concluded that: (1) some pre-existing curvature must have been present before the Late Cretaceous; (2) the orocline acquired part of its curvature after the Paleocene and before the Middle Eocene as a result of South Armenian Block–Eurasia collision; and (3) about 50% of the curvature formed after the Eocene and probably before the Late Miocene, probably as a result of Arabia–Eurasia collision.

Supplementary material: Results from rock magnetic experiments, reversal and fold tests and equal area projections of the characteristic remanent magnetizations for each site, as well as biostratigraphic ages and a table with palaeomagnetic results from the literature review (with assigned numbers referred to in the text) are available at http://www.geolsoc.org.uk/SUP18852.

The Eastern Pontides–Lesser Caucasus fold–thrust belt (Fig. 1a) forms part of the former Eurasian margin that deformed as a result of ongoing Africa(–Arabia)–Eurasia convergence. The peculiar arc-shaped geometry of the Eastern Pontides–Lesser Caucasus, which is expressed in the change
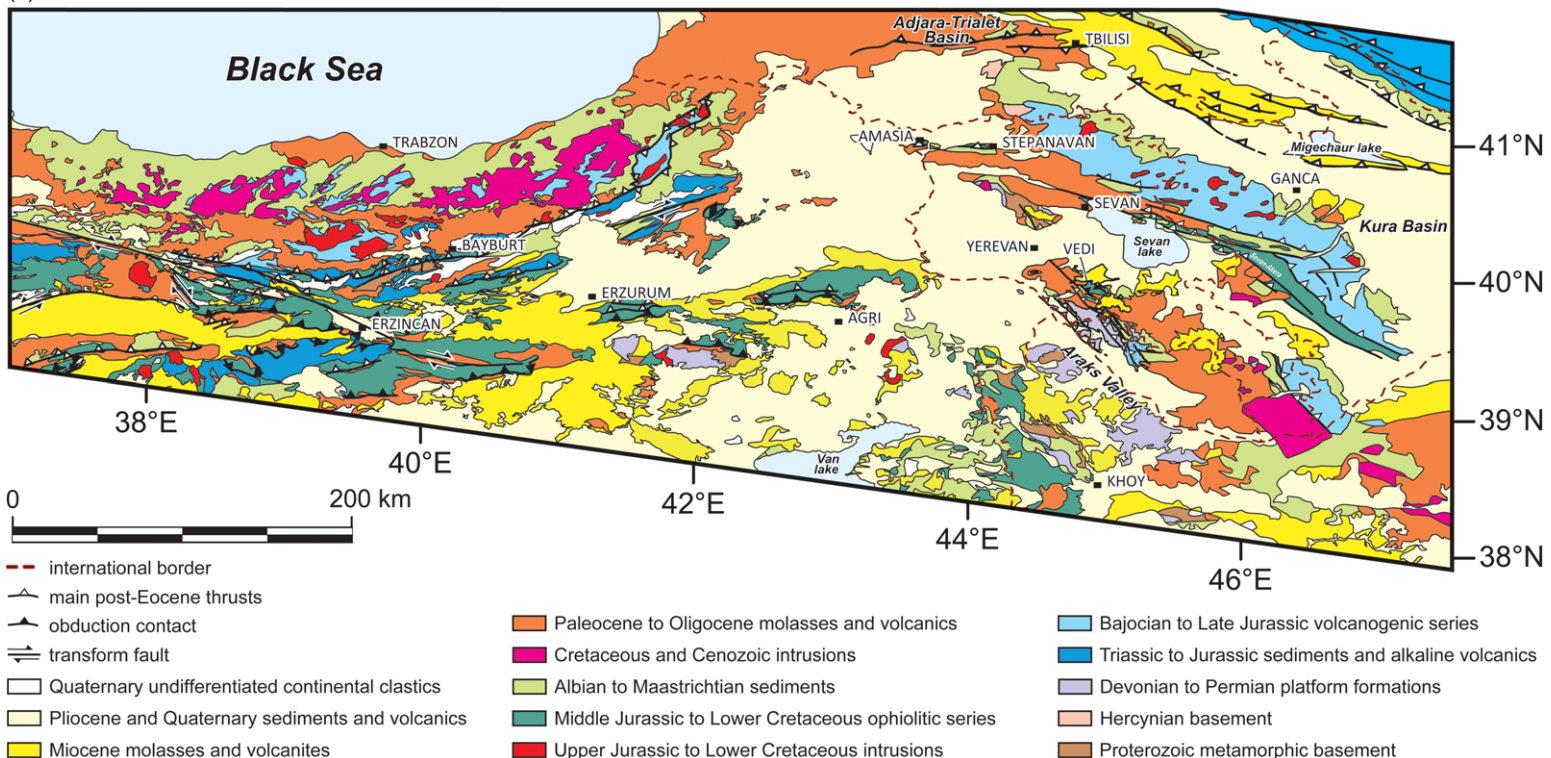
of strike of folds and thrusts, typifies a wider region from the Central Pontides to the Talysh and Alborz mountain belts (see red broken line, Fig. 1a). Based on palaeomagnetic data (Bazhenov & Burtman 2002; Hisarli 2011), the northwards arc-shaped geometry in the Central Pontides is an orocline – a bend imposed on a pre-existing, formerly linear orogenic belt (Carey 1955). To the west, the Central Pontides orocline was formed in the latest Cretaceous to Paleocene as a result of the accretion of the Central Anatolian Crystalline Complex to the (rheologically contrasting) Eurasian margin (Meijers *et al.* 2010; Lefebvre *et al.* 2013). Likewise, the arcuate fold–thrust belts of the Talysh and Alborz ranges could have formed by the indentation of the Arabian plate into the South Caspian Basin
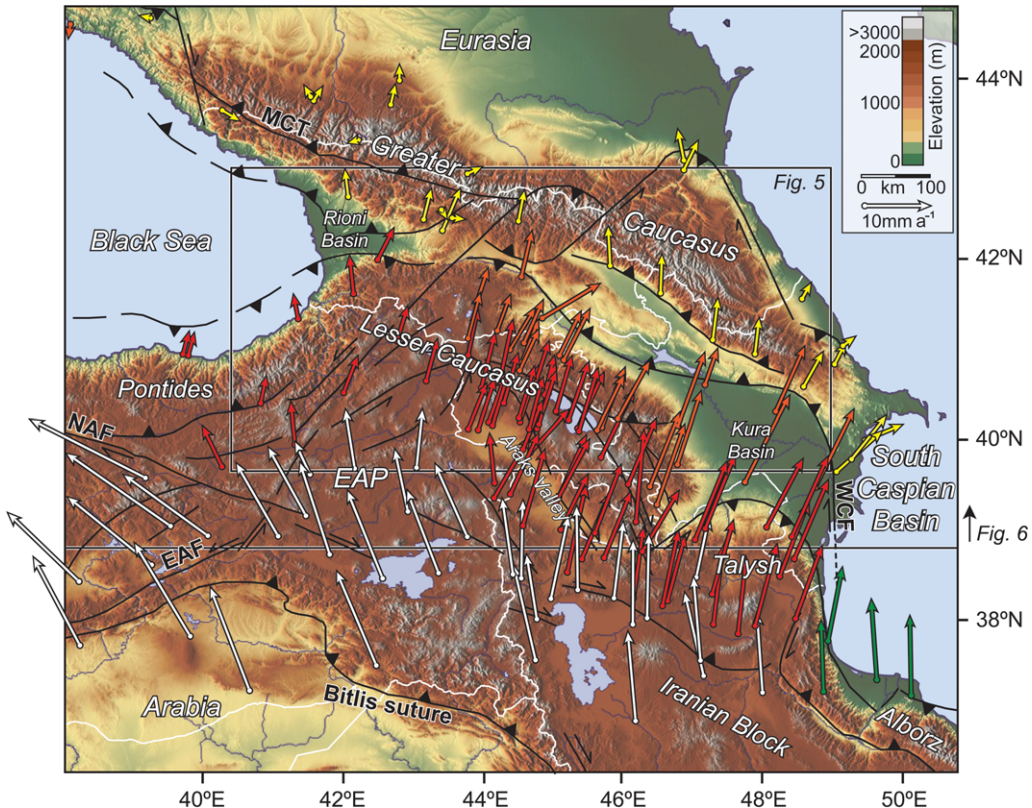
(Agard *et al.* 2011) or as a result of strong contrasts in rheology between the South Caspian Basin (Fig. 2) and the Talysh and Alborz ranges (Fig. 1a; Allen *et al.* 2003). The latter was confirmed for the Alborz range by Cifelli *et al.* (2015), who determined that orocline formation was initiated after *c.* 7.6 Ma (Late Miocene). The Eastern Pontides– Lesser Caucasus fold–thrust belt, the subject of this study, was defined as an orocline based on palaeomagnetic data from Upper Cretaceous and Eocene deposits (Bazhenov & Burtman 2002; Hisarli 2011). In their compilations, Bazhenov & Burtman (2002) and Hisarli (2011) did not find any significant difference in the vertical axis rotations between their Late Cretaceous and Eocene data. Consequently, they pooled these together and


Fig. 1. (**a**) Tectonic map of the Black and Caspian Sea region. AF, Araks Fault; ASHS, AmasiaSevanHakari Suture; ATB, Anatolide–Tauride Block; CACC, Central Anatolian Crystalline Complex; CAF, Central Anatolian Fault; EAF, East Anatolian Fault; Ist. Z., Istanbul Zone; IAES, Izmir–Ankara–Erzincan Suture; GC, Greater Caucasus; MM, Menderes Massif; NAF, North Anatolian Fault; R, Lake Rezaiyeh; SAB, South Armenian Block; SSZ, Sanandaj–Sirjan Zone; TC, Transcaucasus; V, Lake Van. Broken red line roughly indicates the general strike and the strike of the fold axes in the Central Pontides, Eastern Pontides–Lesser Caucasus, Talysh and Central Alborz Mountains fold–thrust belts. Black circular arrows in the Central Pontides, Eastern Pontide–Lesser Caucasus and Central Alborz Mountains indicate the sense of rotation in both limbs of the orocline. The Anatolide–Tauride Block, Istanbul Zone, Sakarya, South Armenian Block and Transcaucasus refer to basement units. Modified after Avagyan *et al.* (2005) and Sosson *et al.* (2010). (**b**) Structural map of the Lesser Caucasus–Eastern Pontides–Northeast Anatolides regions after Hässig *et al.* (2014*a*).

Fig. 1. *Continued.*

Fig. 2. Shaded relief digital elevation model of the Arabia–Eurasia collision zone in the Black and Caspian Sea area. Global positioning system (GPS) velocity vectors from the studies of Reilinger *et al.* (2006), Kadirov *et al.* (2008), Djamour *et al.* (2010, 2011) and Karakhanyan *et al.* (2013) are shown relative to fixed Eurasia. The GPS vectors are colour coded by region (yellow, Greater Caucasus; orange, Kura Basin; red, Lesser Caucasus; white, Arabia, the Iranian and Anatolian plateaus; green, Alborz). Representation of GPS data after Avdeev & Niemi (2011) and major fault zones after Avagyan *et al.* (2010). EAF, East Anatolian Fault; EAP, Eastern Anatolian Plateau; MCT, Main Caucasus Thrust; NAF, North Anatolian Fault; WCF, West Caspian Fault.

concluded that oroclinal bending occurred after Late Cretaceous to Eocene times, but without really quantifying the oroclinal test. No data from younger deposits were presented in either study and therefore the timing as well as the cause of the vertical axis rotations remains unconstrained. Orocline formation could have resulted from two latest Cretaceous and younger major deformation events: (1) the collision of the South Armenian Block (SAB) with the Eurasian margin (i.e. the Transcaucasus basement; Fig. 1a); and (2) the collision of Arabia with the Eurasian margin. Estimates of the age of SAB–Eurasia collision range from the end of the Campanian (Rolland *et al.* 2012) to Paleocene–Eocene (Robinson *et al.* 1995; Okay & Şahintürk 1997; Sosson *et al.* 2010; Robertson *et al.* 2014). A palaeolatitude study on SAB and Eurasian margin sediments (Meijers *et al.* 2015) could not distinguish between the

collision ages proposed by Rolland *et al.* (2012) and Sosson *et al.* (2010). Arabia–Eurasia collision estimates vary widely and range from the Late Cretaceous to Early Miocene, although most researchers agree that collision started during or after the latest Eocene (e.g. Berberian & King 1981; Axen *et al.* 2001; Allen *et al.* 2004; Ritz *et al.* 2006; Guest *et al.* 2007; Vincent *et al.* 2007; Allen & Armstrong 2008; Ballato *et al.* 2011; Mouthereau 2011; Rezaeian *et al.* 2012; Madanipour *et al.* 2013).

Constraining the age of oroclinal bending may therefore enable speculation about which of these collisional events (i.e. SAB–Eurasia or Arabia–Eurasia collision) was responsible for orocline formation. To constrain the timing of oroclinal bending in the Eastern Pontides–Lesser Caucasus fold–thrust belt, we sampled 37 new sites in rocks of Late Cretaceous to Late Miocene age in the Lesser

Caucasus (Georgia and Armenia) for palaeomagnetic analysis. We combined our new data with a compilation of existing data from Cretaceous to Pleistocene strata in the area of interest – including northeastern Turkey, Georgia and Armenia – from the International Association of Geomagnetism and Aeronomy Global Paleomagnetic (GPMDB) Database (http://www.ngu.no/geodynamics/gpmdb/). The data from the GPMDB are often of unknown quality and, in some cases, the data have not been published, which led Bazhenov & Burtman (2002) to exclude all GPMDB data from their review. We included all *c.* 100 of these datasets in our review and applied a number of reliability criteria. The data that were accepted after applying these criteria were taken into account for further analysis. If a coherent temporal and spatial declination pattern emerges from such a large amount of data, it can be assumed that the data must have regional tectonic significance.

Geology of the Eastern Pontides and Lesser Caucasus

The geological and tectonic history of the Caucasus, situated between the Black Sea to the west and the Caspian Sea to the east (Fig. 1a), is mainly determined by its position between the still-converging Eurasian and African–Arabian lithospheric plates within a wide zone of continent–continent collision. During the Late Palaeozoic to Early Cenozoic, the region belonged to the now-vanished Tethys ocean and its southern Eurasian and northern Gondwana margins. Within the Africa–Eurasia convergence zone, a system of island arcs, intra-arc rifts and back-arc basins formed. Microplates drifted from the African margin in the south and accreted to the Eurasian margin in the north following the successive opening and closure of the oceanic domains of the Proto-Tethys, Palaeo-Tethys and finally Neo-Tethys ocean (e.g. Kazmin *et al.* 1986; Ustaömer & Robertson 2010; Adamia *et al.* 2011). During the collisional stages of the late Alpine tectonic cycle resulting from Arabia–Eurasia collision, back-arc basins were inverted into the fold–thrust belts of the Greater and Lesser Caucasus (Fig. 2; Forte *et al.* 2010; Vincent *et al.* 2014). In the west and east, the Rioni and Kura Basins separate the Greater and Lesser Caucasus (Fig. 2; Adamia *et al.* 2011).

Geographically, the Lesser Caucasus is the mountain belt running through Georgia, Armenia and Azerbaijan south of the Kura and Rioni basins and roughly north of the Araks Valley (Fig. 2). Across the Georgian–Turkish border in the west, it continues into the Eastern Pontides. North of the Izmir–Ankara–Erzincan and Amasia–Sevan–Hakari suture zones (Fig. 1a), the basement units

underlying the Eastern Pontides–Lesser Caucasus fold–thrust belt are the Sakarya Zone and the Transcaucasus. South of the Izmir–Ankara–Erzincan and Amasia–Sevan–Hakari suture zones, the basement is formed by the Anatolide Tauride Block and SAB of Pan-African affinity (e.g. Belov & Sokolov 1973; Kröner & Şengör 1990). The Sakarya Zone and the Transcaucasus terranes accreted to the Eurasian margin in the Palaeozoic (Saintot *et al.* 2006; Okay 2008), whereas the SAB of Pan-African affinity started colliding with the Eurasian margin either in the Late Cretaceous (Rolland *et al.* 2012) or in the Paleocene–Eocene (Robinson *et al.* 1995; Okay & Şahintürk 1997; Sosson *et al.* 2010; Robertson *et al.* 2014).

The Sakarya and Transcaucasus terranes (Fig. 1a) are often treated separately, which is probably due to their division over several countries: Turkey in the west (Eastern Pontides) and three former Soviet countries in the east (Georgia, Armenia and Azerbaijan; Lesser Caucasus). The Sakarya and the Transcaucasus basements are both limited by the Scythian Platform (i.e. the thinned margin of the East European Platform) to the north (Yılmaz *et al.* 2000; Hässig *et al.* 2014a).

The northwards drift of Africa led to the collision of its Arabian promontory with Eurasia. Thermochronometric studies by Vincent *et al.* (2007) and Madanipour *et al.* (2013) provide evidence for Early Oligocene Arabia–Eurasia collision in the Western Greater Caucasus and Talysh mountains, respectively, close to our study area. Ongoing convergence in the region is one of the driving forces for the westwards escape of the Anatolian microplate along the North Anatolian Fault (Fig. 1a; Dewey & Şengör 1979; Şengör *et al.* 1985) and continuing deformation in the Lesser and Greater Caucasus (Jackson 1992). The global positioning system (GPS) velocity vectors in the collision zone between Arabia and Eurasia (Fig. 2) show the decoupling of Anatolia and the (Eastern) Pontides–Lesser Caucasus, as well as the large amount of deformation that is being accommodated along the major thrust faults of the Greater Caucasus and the Kura Basin (e.g. Jackson 1992; Forte *et al.* 2010, 2013; Mosar *et al.* 2010). The increase in GPS velocity from west to east across the Lesser Caucasus clearly shows the present-day counter-clockwise (CCW) rotation of the Lesser Caucasus with respect to fixed Eurasia (Reilinger *et al.* 2006; Kadirov *et al.* 2008; Djamour *et al.* 2011; Karakhanyan *et al.* 2013).

The basement units of the Eastern Pontides portion of the Sakarya Zone and the Transcaucasus are covered by unmetamorphosed Late Palaeozoic, Mesozoic and Cenozoic sequences (Fig. 1b; Okay & Şahintürk 1997; Yılmaz & Kandemir 2006; Yılmaz *et al.* 2000; Adamia *et al.* 2011). Widespread Jurassic to Late Cretaceous (Maastrichtian) volcanics are

interpreted as arc volcanics attributable to the north-wards subduction of the Neo-Tethys (Tüysüz *et al.* 1995; Okay & Şahintürk 1997; Tüysüz 1999; Okay *et al.* 2006; Rice *et al.* 2006; Tüysüz & Tekin 2007; Adamia *et al.* 2011). Subduction resulted in high-pressure metamorphism between 170 and 90 Ma (Rolland *et al.* 2009a; Topuz *et al.* 2013).

The metamorphic basement of the SAB (Fig. 1b) mainly consists of gneisses, mica schists and diorite–leucogranite intrusions (Aghamalyan 1998), which record a Late Jurassic to Early Cretaceous (160–120 Ma) metamorphic evolution in response to the south-dipping subduction of the Neo-Tethys below the SAB (Hässig *et al.* 2014b). The basement rocks are unconformably overlain by unmetamor-phosed incomplete Palaeozoic to Mesozoic (Santonian) sedimentary sequences (Paffenholtz 1959; Karyakin 1989; Sosson *et al.* 2010). These sedimentary sequences are overlain by Middle to Upper Jurassic ophiolitic sequences (Danelian *et al.* 2008, 2010, 2012; Galoyan *et al.* 2009; Rolland *et al.* 2009b; Asatryan *et al.* 2012; Hässig *et al.* 2013), which are, in turn, unconformably overlain by oceanic island basalts and arc-type volcanic rocks (Galoyan *et al.* 2007, 2009; Galoyan 2008) of Early Cretaceous age (Belov *et al.* 1991; Rolland *et al.* 2011; Asatryan *et al.* 2012). Santonian and younger sedimentary, volcano-sedimentary and volcanic rocks cover the ophiolites, oceanic island basalts and arc-type volcanic rocks (Sosson *et al.* 2010).

Strike test
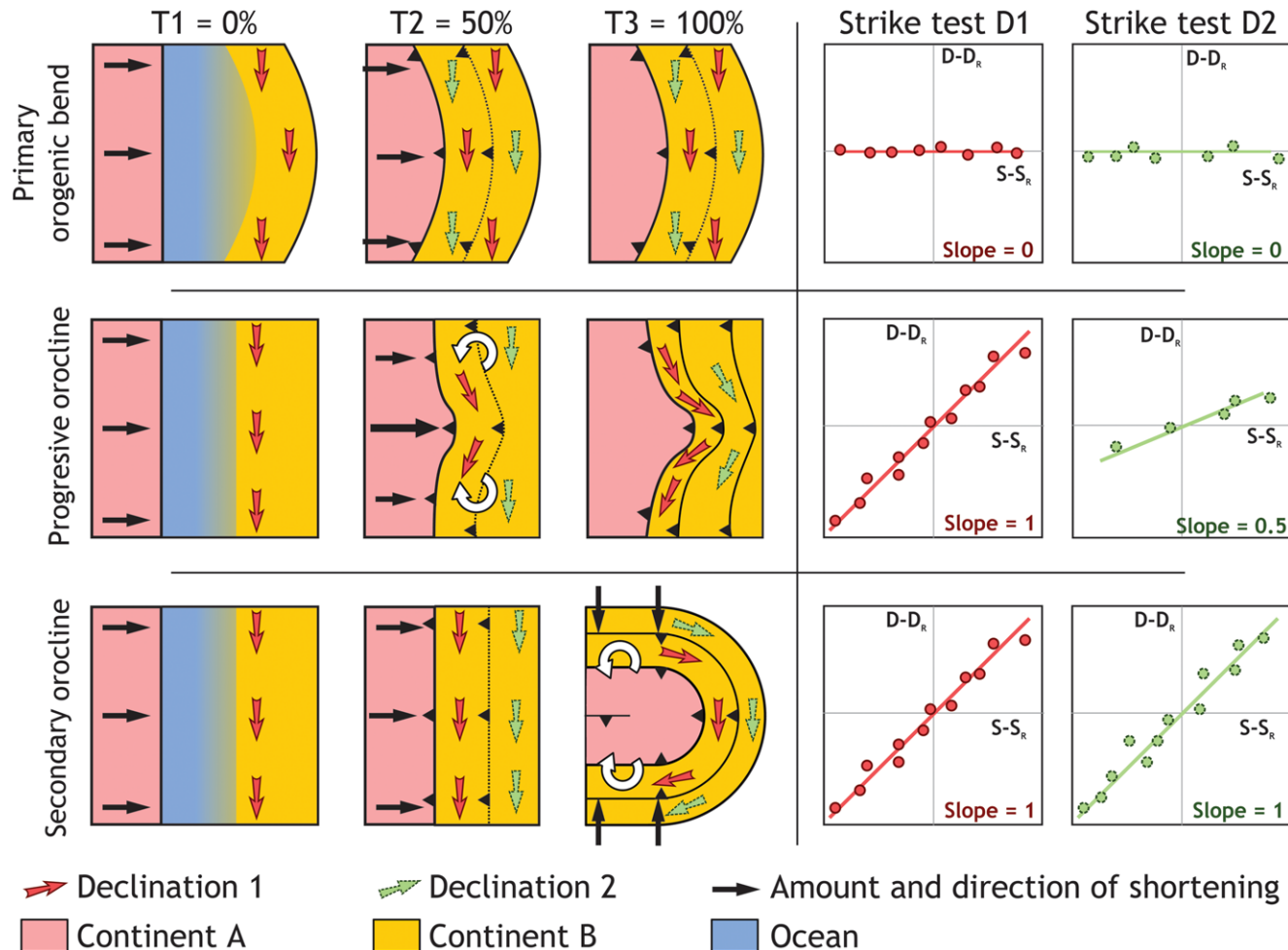
Orogenic bends are classified based on kinematics and the relative timing of curvature (Weil & Sussman 2004; Johnston *et al.* 2013). Orogens and thrust belts characterized by primary bends are those in which the curvature is an inherited physiographical feature present prior, during and throughout the formation of the orogen, such as an embayment. Oroclines are map-view curves that developed in response to the bending or buckling of an existing orogenic belt about a vertical axis of rotation (Carey 1955). The strike test (or orocline test; Schwartz & Van der Voo 1983; Eldredge *et al.* 1985; Yonkee & Weil 2010) evaluates the relationship between variations in the regional structural trend and the orientations of given geological fabric elements (e.g. palaeomagnetic declinations, fractures, cleavage, veins or lineations). The strike test distinguishes between two end-members: (1) a primary arcuate shape of a mountain belt that yields no variation of declination with strike, resulting from the absence of vertical axis rotations; and (2) a secondary orocline, characterized by a unit slope relation between the declination and the structural grain. Any intermediate relation between both

parameters is known as a progressive orocline and could indicate one of two scenarios. In the first scenario, a partial initial curvature of the fold–thrust belt existed, which was modified by a later tectonic event. Alternatively, in the second scenario, the sampled rocks acquired their magnetization during the process of oroclinal bending, due either to remagnetization or to their formation during oroclinal bending. The two end-members and the intermediate field are illustrated in declination v. strike plots of the fold axis diagram in Figure 3. Our new data and the previously published data presented in this study were assessed using the strike test.

This study

Sampling and experimental procedure

The goal of this study was to constrain the timing of rotation previously observed by Bazhenov & Burtman (2002) and Hisarli (2011) in Upper Cretaceous and Eocene rocks. We therefore attempted to sample Oligocene to Pliocene geological formations. The mostly coarse, clastic Neogene rocks were, however, often weathered and/or unsuitable for palaeomagnetic sampling. In the Georgian and Armenian segments of the Eastern Pontides–Lesser Caucasus orocline, we collected a total of 734 oriented palaeomagnetic cores from 37 sites (Table 1) using a gasoline-powered motor drill. The sampling covered four areas along the curvature of the belt. In Georgia, 15 sites east and west of Tbilisi, six sites in the Akhaltsikhe area and seven sites close to Batumi were sampled. In Armenia, nine sites were sampled in or just north of the SAB (Table 1). In terms of age and lithology, our dataset included four sites in Upper Cretaceous–Paleocene limestones and silty marls, 20 sites in Eocene siltstones, turbidites, tuffs and (volcano-)clastic sediments, five sites in Oligocene (carbonatic) clay/siltstones and eight sites in Miocene mud/silt/sandstones, limestones and tuffs (Table 1). Ages were assigned based on nannofossils, molluscs, ostracods, forams or a combination of these species (Sadradze 2015). Only the age of site BB was derived from the geological map. Core orientations were measured with a magnetic compass and corrected for *c.* 6° present-day declination. Whenever permitted by their length, the cores were cut into multiple specimens in the laboratory. Subsequently, specimens were: (1) thermally demagnetized in a magnetically shielded oven ($n = 335$); (2) alternating field (AF) demagnetized ($n = 83$); or (3) thermally demagnetized up to 150 or 190°C followed by AF demagnetization ($n = 461$). We refer to the last group (combined thermal and AF demagnetization) as AF demagnetized, as the characteristic remanent magnetization (ChRM) was mostly isolated

Fig. 3. Figure illustrating two end-members (primary orogenic bend v. secondary orocline) and an intermediate field (progressive orocline). T1, T2 and T3 are arbitrary successive moments in time. D, declination; D_R, reference declination; S, strike; S_R, reference strike.

Table 1. *Palaeomagnetic results from this study*

Site	Rock type	Site lat.	Site long.	S	Age*	ΔAge	N_{samp}	N_{af}
Eurasian margin								
Area east of Tbilisi								
GE01	**Siltstones**	**41.82 028**	**45.13658**	**81**	**11.5**	**0.5**	**16**	**18**
GE04	**Red silty mudstones**	**41.45679**	**45.36972**	**130**	**11.5**	**0.5**	**12**	**6**
GE02	Siltstones	41.80948	45.14274		11.0	1.0	19	20
GE03	**Marls, oolites and carbonatic silt/ sandstones**	**41.77736**	**45.14838**	**91**	**11.5**	**0.5**	**19**	**24**
GE14	Pseudo marine oolithic limestones, carbonate and sandstone layers	41.83564	44.86601		13.8	2.2	20	8
Area west of Tbilisi								
GE12	**Volcanoclastics**	**41.91448**	**44.09559**	**96**	**39.7**	**1.7**	**20**	**20**
GE13	**Siltstones and sandstones**	**41.93221**	**44.10476**	**107**	**33.9**	**0.9**	**19**	**18**
GE11	**Silty marls and fine siltstones**	**41.95531**	**44.32219**	**82**	**29.9**	**4.0**	**20**	**17**
GE06	Turbidite succession	41.66471	44.39996		45.0	11.1	15	16
GE05	**Turbidite succession**	**41.65903**	**44.41413**	**88**	**36.0**	**0.8**	**14**	**13**
GE10	**White oolithic limestones, light beige limestones and grey marls**	**41.89856**	**44.44140**	**128**	**11.0**	**0.5**	**25**	**9**
GE07	**Turbiditic section of tuffs, epiclastics and volcanics**	**41.63924**	**44.45705**	**88**	**42.9**	**4.9**	**13**	**6**
GE08	**Turbiditic section of tuffs, epiclastics and volcanics**	**41.63653**	**44.46086**	**88**	**39.7**	**1.7**	**16**	**16**
GE15	**Carbonatic siltstones**	**41.77411**	**44.70181**	**88**	**29.9**	**4.0**	**20**	**22**
GE09	**Marls, limestones and mudstones**	**41.61774**	**44.50652**	**90**	**67.7**	**1.5**	**18**	**17**
Akhaltsikhe region								
GE20	Terrigenous clastics, carbonaceous siltstones and sandstones	41.65343	42.94237		36.0	2.1	21	8
GE18	**Epiclastics**	**41.60743**	**43.04279**	**76**	**36.0**	**0.8**	**20**	**19**
GE19	**Volcanic tuff, dacitic composition**	**41.57747**	**43.09700**	**75**	**8.2**	**0.1**	**19**	**21**
GE21	**Volcanic tuff, dacitic composition**	**41.57882**	**43.11946**	**75**	**8.2**	**0.1**	**22**	**19**
GE17	**Marine clastic turbidites**	**41.60399**	**43.14416**	**50**	**44.4**	**2.0**	**21**	**17**
GE16	**Basaltic turbidites**	**41.57407**	**43.30937**	**52**	**44.4**	**2.0**	**19**	**12**
Batumi region								
GE22	Basaltic turbidites	41.55490	41.80330		42.9	4.9	21	11
GE23	**Volcanoclastic turbidites**	**41.57080**	**41.85160**	**60**	**36.0**	**0.8**	**26**	**25**
GE28	Limestones and marls	42.06820	42.05591		67.7	1.5	22	10
GE26	Claystones	41.95736	42.12228		28.5	5.4	20	9
GE24	Volcanoclastic turbidites	41.63415	42.15942		36.0	0.8	9	8
GE27	**Submarine volcanoclastics and epiclastics**	**41.95848**	**42.22464**	**66**	**36.0**	**2.1**	**20**	**19**
GE25	Basaltic turbidites	42.06932	42.26331		38.3	1.5	19	9
South Armenian Block								
BB	Deltaic and lacustrine floodplain sediments	40.90103	43.81350		45.0	11.1	37	0
BA	Limestones	40.48182	45.42365		84.2	0.8	30	8
BK	**Dark grey siltstones**	**39.94216**	**44.82061**	**135**	**38.3**	**1.5**	**24**	**27**
AA	**Volcano-detrital marine Silt/sandstones**	**39.93826**	**44.86673**	**135**	**38.3**	**1.5**	**25**	**13**
AB	**Silty marls, siltstones and mudstones**	**39.93826**	**44.86673**	**137**	**59.8**	**0.6**	**18**	**10**
BE	**Sandstones/siltstones/marls, samples taken from siltstones**	**39.97592**	**44.87509**	**135**	**38.3**	**1.5**	**18**	**12**
BH	**Silty marls and limestones, samples from limestones**	**39.80913**	**45.06853**	**135**	**36.0**	**0.8**	**21**	**19**
BG	**Alteration of marly siltstones, siltstones and coarse sandstones**	**39.73702**	**45.25127**	**135**	**38.3**	**1.5**	**21**	**18**
BD	**(Volcano)clastics and turbidites**	**39.72083**	**45.54520**	**135**	**38.3**	**1.5**	**15**	**20**
						Sum:	734	544

		ChRM directions – in situ									ChRM directions – tilt corrected				
N_{th}	N_{gc}	N/N_{45}	DEC	ΔD_x	INC	ΔI_x	k	α_{95}	K	A_{95}	N/N_{45}	DEC	ΔD_x	INC	ΔI_x
11	8	11/11	127.5	13.2	69.2	5.5	86.9	4.9	34.0	7.9	11/11	15.7	5.7	48.1	5.8
6	1	12/12	349.4	7.8	66.5	7.8	33.9	7.6	17.7	10.6	12/12	18.4	6.8	28.5	10.9
6															
12	12	15/15	262.6	43.8	− 81.1	6.4	36.6	6.7	12.0	11.9	15/15	189.1	8.9	− 44	10.1
6		11/8	17.6	35.2	66.9	16.1	15.3	14.6	7.3	22.0	11/9	8.7	13.0	2.5	26.0
7	8	15/15	50.7	19.0	− 68.2	8.3	25.4	7.7	11.6	11.7	15/15	182.7	9.9	− 42.2	11.9
12	7	11/11	9.0	24.7	− 67.0	11.4	18.5	10.9	9.4	15.7	11/11	190.3	14.3	− 44	16.6
11	6	10/10	20.3	19.3	74.4	5.7	86.5	5.2	28.0	9.3	10/10	358.2	4.8	51.4	4.4
6	0	15/10	16.7	18.4	62.4	18.4	8.3	17.9	5.6	22.4	15/7	180.1	13.0	44.7	13.0
8	5	8/8	264.7	12.7	− 61.4	7.9	65.3	6.9	36.0	9.4	8/8	190.1	8.0	− 48	8.2
5	0	18/17	4.0	12.5	59.3	8.5	26.4	7.1	15.0	9.5	18/17	21.5	8.1	43.5	9.5
11	2	11/11	20.1	8.2	26.2	13.6	24.2	9.5			11/11	9.2	8.0	52.0	7.2
7	0	7/7	311.7	19.6	− 62.9	11.2	38.0	9.9	19.9	13.9	7/7	185.5	12.1	− 47	12.6
10	7	10/10	180.4	20.2	71.7	7.1	56.0	6.5	20.3	11.0	10/10	6.5	9.2	50.9	8.6
6	0	4/3	211.0	23.6	60.1	15.4	65.3	15.4	50.0	17.6	13/13	34.7	7.4	37.0	10.1
		9/9	321.8	12.2	54.6	10.0	41.9	8.1	27.7	10.0					
12	0	8/10	247.3	24.1	−48.1	24.5	9.9	18.5	7.9	20.9	9/10	227.1	19.2	−28.0	30.9
8	0	22/21	96.5	18.1	− 73.0	5.9	33.0	5.6	12.6	9.3	22/22	149.2	6.1	− 38	8.3
8	1	29/29	348.6	2.5	31.1	3.9	80.1	3.0	124.4	2.4	29/29	355.7	2.8	37.1	3.7
5	0	23/23	327.2	12.6	65.2	6.5	27.8	5.8	13.7	8.5	23/23	5.3	5.7	35	8.1
8	3	8/8	156.2	10.7	− 30.1	16.7	34.6	9.6	30.1	10.3	8/8	159.9	14.5	− 52	12.9
8	8	18/18	196.6	7.7	− 53.0	6.7	46.0	5.2	30.2	6.4	18/18	181.2	5.2	− 31	8.0
14	0	18/18	9.5	5.7	60.7	3.7	104.4	3.4	67.1	4.3	18/18	26.4	2.6	6.6	5.2
8	5	25/25	152.2	4.6	− 13.8	8.8	24.6	6.0	41.0	4.6	25/25	155.8	5.9	− 39	7.7
14	1	7/5	341.5	33.8	35.9	46.8	5.9	34.5	6.8	31.5	7/5	356.3	46.1	54.9	35.8
12	0	7/6	356.1	30.6	45.7	33.1	7.0	27.2	7.1	26.9	7/4	83.8	24.7	54.2	20.3
5	8	12/12	349.5	16.8	62.1	10.1	26.7	8.6	13.7	12.2	12/12	347.9	9.8	40.2	12.5
8	8	16/15	284.0	10.9	− 54.8	8.9	29.9	7.1	19.5	8.9	16/16	168.5	8.7	− 40	11.1
14	0	13/11	182.5	10.8	− 2.7	21.7	8.0	17.2	18.7	10.8	11/11	182.3	14.2	30.2	22.1
7	0	6/3	11.6	19.1	61.0	12.0	152.2	10.0	77.6	14.1	6/3	203.5	99.9	73.8	24.7
10	1	14/14	200.6	9.8	− 29.4	15.5	13.4	11.3	18.7	9.7	14/13	197.9	15.9	− 55.1	12.8
14	7	31/31	358.5	4.2	4.2	8.3	28.4	4.9	39.5	4.2	31/31	2.5	7.2	51.6	6.6
14	19	26/26	213.6	4.2	− 14.5	8.0	41.3	4.5	46.6	4.2	26/26	210.7	3.9	− 35	5.6
11	19	21/20	241.6	6.5	42.8	7.8	31.5	5.9	31.2	5.9	21/20	225.4	5.6	− 25	9.3
6	10	18/17	208.8	8.4	0.7	16.7	16.3	9.1	19.2	8.4	18/17	206.4	9.4	− 26.4	15.6
12	0	31/31	190.8	4.4	− 27.5	7.1	31.9	4.6	38.6	4.2	31/31	191.3	4.9	− 35.5	6.9
6	0	19/19	156.0	11.6	− 74.3	3.4	97.5	3.4	36.5	5.6	19/19	194.9	3.4	− 29.9	5.3
7	0	14/14	200.9	5.7	− 28.8	9.1	35.0	6.8	53.1	5.5	14/14	195.9	10.5	− 59.0	7.3
335															

(*Continued*)

Table 1. *Continued.*

Site	Rock type	λ	k	α₉₅	K	A₉₅	LT/ LCF component – in situ				
							N/N_{45}	DEC	ΔD_x	INC	ΔI_x
Eurasian margin											
Area east of Tbilisi											
GE01	**Siltstones**	**29.1**	**120.2**	**4.2**	**84.4**	**5.0**	**24/24**	**0.5**	**4.0**	**60.0**	**2.7**
GE04	**Red silty mudstones**	**15.2**	**33.8**	**7.6**	**44.7**	**6.6**					
GE02	Siltstones										
GE03	**Marls, oolites and carbonatic silt/sandstones**	**25.8**	**31.5**	**6.9**	**23.8**	**8.0**	**22/22**	**1.2**	**2.8**	**57.1**	**2.1**
GE14	Pseudo marine oolithic limestones, carbonate and sandstone layers	1.2	11.5	15.9	16.6	13.0					
Area west of Tbilisi											
GE12	**Volcanoclastics**	**24.4**	**25.4**	**7.7**	**18.9**	**9.0**	**24/22**	**359.1**	**8.6**	**57.3**	**6.4**
GE13	**Siltstones and sandstones**	**25.3**	**18.3**	**11.0**	**13.5**	**12.9**	**16/16**	**359.9**	**3.9**	**61.8**	**2.4**
GE11	**Silty marls and fine siltstones**	**32.0**	**201.9**	**3.4**	**143.6**	**4.0**	**11/11**	**0.6**	**5.9**	**57.2**	**4.4**
GE06	Turbidite succession	26.4	28.9	11.4	27.9	11.6					
GE05	**Turbidite succession**	**28.9**	**68.7**	**6.7**	**63.6**	**7.0**	**17/17**	**0.1**	**2.6**	**59.7**	**1.8**
GE10	**White oolithic limestones, light beige limestones and grey marls**	**25.4**	**26.5**	**7.1**	**24.6**	**7.3**	**6/6**	**21.4**	**31.7**	**49.1**	**30.9**
GE07	**Turbiditic section of tuffs, epiclastics and volcanics**	**32.6**	**62.3**	**5.8**	**47.4**	**6.7**	**13/13**	**0.4**	**5.3**	**60.3**	**3.5**
GE08	**Turbiditic section of tuffs, epiclastics and volcanics**	**28.5**	**37.4**	**10.0**	**33.3**	**10.6**	**6/5**	**343.8**	**22.5**	**56.1**	**17.3**
GE15	**Carbonatic siltstones**	**31.6**	**62.7**	**6.1**	**39.1**	**7.8**	**15/15**	**0.9**	**4.0**	**58.3**	**2.9**
GE09	**Marls, limestones and mudstones**	**20.6**	**31.8**	**7.5**	**36.4**	**7.0**	**13/13**	**359.1**	**4.6**	**57.6**	**3.3**
Akhaltsikhe region											
GE20	Terrigenous clastics, carbonaceous siltstones and sandstones	14.9	8.0	19.5	8.7	18.5	5/5	1.8	19.9	60.8	12.6
GE18	**Epiclastics**	**21.0**	**26.6**	**6.1**	**30.3**	**5.7**	**21/21**	**11.0**	**11.6**	**58.7**	**8.1**
GE19	**Volcanic tuff, dacitic composition**	**20.7**	**80.1**	**3.0**	**108.8**	**2.6**	**15/12**	**357.6**	**7.6**	**46.9**	**8.0**
GE21	**Volcanic tuff, dacitic composition**	**19.3**	**27.9**	**5.8**	**32.6**	**5.4**					
GE17	**Marine clastic turbidites**	**32.7**	**37.3**	**9.2**	**21.8**	**12.1**	**2/2**	**20.4**		**52.2**	
GE16	**Basaltic turbidites**	**16.9**	**44.0**	**5.3**	**48.7**	**5.0**	**12/9**	**16.2**	**16.8**	**60.4**	**10.9**
Batumi region											
GE22	**Basaltic turbidites**	3.3	104.1	3.4	172.2	2.6	6/6	22.2	30.7	53.7	25.7
GE23	**Volcanoclastic turbidites**	**22.2**	**24.5**	**6.0**	**28.9**	**5.5**	**8/8#**	**2.3**	**7.5**	**56.8**	**5.7**
GE28	Limestones and marls	35.4	6.8	31.7	5.5	35.9	11/9	349.9	23.9	59.6	15.8
GE26	Claystones	34.8	36.2	15.5	22.0	20.1					
GE24	Volcanoclastic turbidites	22.9	26.6	8.6	23.9	9.1	3/3	353.3	99.9	71.6	37.4
GE27	**Submarine volcanoclastics and epiclastics**	**22.4**	**23.1**	**7.8**	**22.2**	**8.0**	**25/25**	**6.3**	**7.9**	**62.8**	**4.6**
GE25	Basaltic turbidites	16.2	9.8	16.2	13.5	13.6	16/15	9.8	13.6	63.0	7.8
South Armenian Block											
BB	Deltaic and lacustrine floodplain sediments	59.9	24.9	25.3	10.5	40.0					
BA	Limestones	35.6	15.7	10.8	11.3	12.9	10/8	350.9	21.4	59.2	14.5
BK	**Dark grey siltstones**	**32.2**	**28.2**	**4.9**	**19.0**	**6.1**	**31/24**	**354.0**	**15.5**	**68.1**	**6.8**
AA	**Volcano-detrital marine Silt/sandstones**	**19.3**	**56.8**	**3.8**	**58.8**	**3.7**	**27/27**	**349.3**	**4.5**	**54.8**	**3.6**
AB	**Silty marls, siltstones and mudstones**	**13.4**	**32.3**	**5.8**	**38**	**5.4**	**21/21**	**355.9**	**5.6**	**58.8**	**3.9**
BE	**Sandstones/siltstones/marls, samples taken from siltstones**	**14.0**	**16.3**	**9.1**	**16.2**	**9.1**	**18/16**	**355.8**	**10.6**	**60.1**	**7.0**
BH	**Silty marls and limestones, samples from limestones**	**19.7**	**30.5**	**4.8**	**31.9**	**4.6**	**13/13**	**4.0**	**10.9**	**57.0**	**8.2**
BG	**Alteration of marly siltstones, siltstones and coarse sandstones**	**16.0**	**96.9**	**3.4**	**106.3**	**3.3**	**19/17**	**7.0**	**9.6**	**62.7**	**5.6**
BD	**(Volcano)clastics and turbidites**	**39.7**	**35.0**	**6.8**	**25.2**	**8.1**	**15/19**	**7.6**	**11.6**	**61.4**	**7.2**

Site lat., Site latitude; Site long., Site longitude; S, regional strike trend at the sampling location, ΔAge, age error; N_{samp}, number of of demagnetization diagrams for which the great circle approach was used to determine the ChRM; N/N_{45}, total number of determined (VGPs); DEC, declination; INC, inclination; ΔD_x and ΔI_x, error in declination (*D*) and inclination (*I*) determined following Butler (1992), tions; *K*, precision parameter determined from the mean VGP directions; A95, cone of confidence determined from the mean VGP criteria in the text.
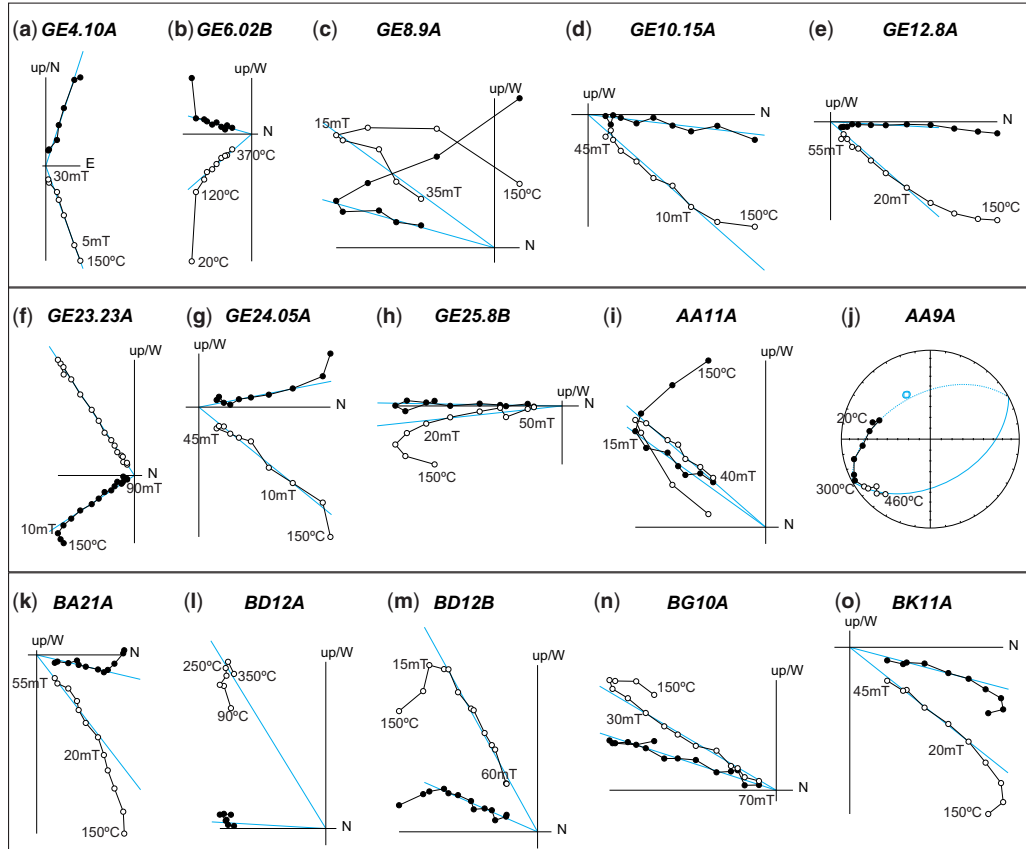
k	α_{95}	K	A_{95}	LT/ LCF component – tilt corrected									Exclusion reason
				N/N_{45}	DEC	ΔD_x	INC	ΔI_x	k	α_{95}	K	A_{95}	
133.3	2.6	95.6	3.0	24/24	356.9	2.0	1.6	4.1	77.1	3.4	209.7	2.0	
													3
284.1	1.8	195.4	2.2	22/22	359.8	2.6	6.9	5.1	61.1	4.0	143.3	2.6	
													2,4
33.7	5.4	12.9	6.8	24/24	10.5	5.4	−6.3	10.7	23.5	6.2	31.2	5.4	
280.2	2.2	164.5	2.9	16/16	5.1	2.3	−0.8	4.6	86.4	4.0	259.4	2.3	
114.7	5.3	97.9	4.6	11/11	355.2	4.7	26.5	7.7	55.7	6.2	101.6	4.6	
													2,3
554.6	1.5	322.8	2.0	17/17	343.4	1.8	12.8	3.3	201.3	2.5	421.7	1.7	
8.7	24.1	7.1	27.1	6/6	29.8	20.6	30.7	31.6	8.7	24.1	12.6	19.7	
146.3	3.4	109.5	4.0	13/13	299.3	25.0	69.1	10.3	18.7	9.8	8.7	14.9	
33.4	13.4	19.3	17.9	6/6	350.5	21.0	1.1	41.9	8.7	24.1	11.1	21.0	
199.6	2.7	151.6	3.1	15/15	1.9	1.7	1.4	3.4	190.6	2.8	501.3	1.7	
180.4	3.1	135.6	3.6	5/5	29.4	4.5	42.6	5.4	236.3	5.0	344.4	4.1	
				8/8	4.7	3.5	−3.3	7.0	84.5	6.1	252.0	3.5	
51.0	10.8	27.9	14.7	5/5	7.1	8.9	36.1	12.3	51.0	10.8	85.2	8.3	5,6
25.3	6.4	13.7	8.9	21/21	0.8	5.4	13.3	10.3	24.3	6.6	35.8	5.4	
48.4	6.3	42.9	6.7	15/12	10.8	8.4	50.6	7.9	48.4	6.3	37.7	7.2	
				2/2	53.0		60.5						
32.4	9.2	17.8	12.6	12/9	356.8	12.0	36.3	16.6	25.9	10.3	21.9	11.3	
6.1	29.4	8.1	25.0	6/5	33.6	13.4	7.9	26.3	32.6	13.6	33.9	13.3	4
87.6	4.6	87.6	6.0	8/8[#]	51.2	10.4	67.9	4.7	152.9	4.5	72.2	6.6	
13.8	14.4	9.2	17.9	11/7	90.4	30.9	58.8	21.1	13.0	7.6	7.6	23.4	2,3
													1,2,3
15.0	33.0	5.6	57.6	3/3	349.2	48.4	49.8	45.0	15.0	33.0	10.6	40.0	2
49.9	4.1	27.0	5.7	25/25	338.8	3.6	−2.1	7.2	41.0	4.6	66.0	3.6	
23.7	8.0	16.6	4.1	16/16	10.9	7.3	26.2	12.2	20.3	8.4	27.8	7.1	3
													1,2,3,4
19.2	13.0	12.5	16.3	10/8	290.6	30.6	70.5	11.4	25.9	11.1	11.4	17.1	5
22.6	6.4	10.4	9.7	31/26	163.8	12.2	54.7	10.0	11.0	9.0	9.0	10.0	
87.5	3.0	59.6	3.6	27/27	308.4	7.7	55.1	6.2	31.9	5.0	20.8	6.2	
78.4	3.6	54.9	4.3	21/21	291.7	6.1	45.9	6.7	50.7	4.5	35.1	5.4	
38.8	6.0	22.2	8.0	18/16	297.1	13.3	64.7	13.3	38.7	6.0	17.3	9.1	
39.9	6.6	24.1	8.6	13/13	3.5	15.4	65.1	8.0	38.0	6.8	16.9	10.4	
56.5	4.8	27.9	6.9	19/19	19.2	5.0	18.5	9.2	27.9	6.5	46.7	5.0	
40.3	6.1	21.2	8.5	19/15	278.6	34.6	79.8	6.0	40.4	6.1	12.9	11.1	

sampled cores; N_{af}, number of alternating field demagnetized specimens; N_{th}, number of thermally demagnetized specimens; N_{gc}, number ChRM directions/remaining number of ChRM directions after application of a fixed 45° cut-off on the virtual geomagnetic poles k, estimate of the precision parameter determined from the ChRM directions; α_{95}, cone of confidence determined from the ChRM directions; λ, calculated palaeolatitude. The numbers in the 'Exclusion reason' column correspond to the numbers of the reliability

from the AF demagnetization steps. Samples were heated to 150–190°C to: (1) remove a viscous remanent magnetization component (often carrying a present-day field direction) commonly recorded in sediments; (2) demagnetize the goetithe (Néel temperature = 120°C; Özdemir & Dunlop 1996) present in a significant number of samples and often carrying the aforementioned viscous remanent magnetization; and (3) remove possible stress in magnetite grains caused by surface oxidation at low temperatures (Van Velzen & Zijderveld 1995). On all sites (except for site BB), both AF and thermal demagnetization were carried out to test the efficiency of each treatment in isolating the ChRM and the reproducibility of the results (e.g. site BD; Fig. 4l–m). Natural remanent magnetization demagnetization is displayed using orthogonal vector diagrams (Zijderveld 1967). The sample ChRM

directions were determined using principal components analysis (Kirschvink 1980) on five to seven successive demagnetization steps for most of the samples. For datasets with low quality demagnetization diagrams, however, this was not always possible. Samples carrying two magnetization components with overlapping unblocking fields (H_{ubs}) or temperatures (T_{dbs}) were analysed using the great circle approach (e.g. Fig. 4j; McFadden & McElhinny 1988). This method determines the direction that lies closest on the great circle to the mean from well-determined natural remanent magnetization directions.

The magnetic mineralogy of representative samples for each site was determined by the interpretation of thermomagnetic runs performed either in low field (0.38 mT) or in high field (150–300 mT) for one or two samples per site. In the

Fig. 4. (**a–o**) Orthogonal vector diagrams (Zijderveld 1967) showing characteristic demagnetization diagrams for the sampled sites. Closed (open) circles indicate the projection on the horizontal (vertical) plane. Alternating field and thermal demagnetization steps are indicated. All diagrams are displayed after correction for bedding tilt. Examples of (1) specimens from the same sample that were alternating field and thermally demagnetized are included for comparison of both techniques for sample BD12 (**l, m**) as well as (2) a specimen (AA9A, **j**) that was interpreted using great circles (see text for explanation).

former case, the susceptibility v. temperature runs (K/T curves) were performed on an Agico KLY-3S Kappabridge, equipped with a CS-L low-temperature device and a CS-3 furnace apparatus at the University of Montpellier II (France). The powdered samples were sieved into $0.125-0.8$ mm grain size fractions. They were first heated from liquid nitrogen (77 K) to room temperature and then heated and cooled in air and/or in argon up to successively higher temperature steps (c. 280, 350, 420, 590 and 700°C) to monitor possible chemical changes in the magnetic minerals. At the end of these cycles, a low-temperature run was repeated on the same powder. In the latter high-field case, powdered samples were placed in a modified horizontal translation type Curie balance with a sensitivity of c. 5×10^{-9} Am^2 (Mullender et al. 1993). A $35-55$ mg mass of powdered rock sample was placed into a quartz glass holder and was held in place by quartz wool. At heating and cooling rates of 10°C/min, the temperatures were cycled up and down up to a maximum temperature of 700°C.

Site means and virtual geomagnetic poles (VGP) and their means were calculated from the ChRM directions. A 45° fixed cut-off was applied on the VGPs per site to remove outliers. The error in declination (ΔD_x) and inclination (ΔI_x) were calculated from the A_{95} value following Butler (1992). Because directional distributions become more elongated towards lower latitudes, this approach more realistically describes the associated errors (Creer et al. 1959; Tauxe et al. 2008; Deenen et al. 2011). Wherever applicable, the reversal test of McFadden & McElhinny (1990) and the fold test of Tauxe & Watson (1994) were carried out.

Rock magnetic results

The rock magnetic data show that the magnetic carriers are similar in the SAB and in the Georgian sites of the Transcaucasus, irrespective of rock type. The magnetic carriers can, however, show large within-site variations with either ferrimagnetic behaviour with a well-defined Curie temperature (T_c, e.g. GE19.17) or only paramagnetic behaviour (e.g. GE21.21) with no T_c. In addition to these paramagnetic curves, several types of thermomagnetic curve can be distinguished. The majority of the data are characterized by reversible (volcanic tuff; e.g. GE19.17) or near-reversible curves (turbidites, volcanoclastics; e.g. GE05 and BD11, respectively) with a single T_c between 520 and 550°C, characteristic of unoxidized low-Ti titanomagnetite. Low-temperature runs down to the LN2 temperature (77 K) confirm the presence of an original magnetic mineral close to magnetite in composition with a Verwey transition around $100-110$ K (-173 to -163°C; e.g. GE05.10). Site GE23 (volcanoclastic

turbidites) shows also almost no alteration up to 500°C, pointing again to a low-Ti titanomagnetite as the original magnetic mineral, but here large transformations occurred when the sample was heated to 700°C. It is probable that some titanomaghemite was initially present, which inverted to hematite, as shown by the irreversibility of the cooling curve. Other curves are characterized by reversible behaviour up to c. 350°C, but a large degree of irreversibility above $400-450$°C (e.g. GE07.07). These curves also show Curie temperatures of magnetite in the range $550-580$°C. Magnetite was originally present in GE07 (turbiditic section of tuffs), as shown by the Verwey transition in the first low-temperature run, probably together with a titanomaghemite that inverted on heating above 330°C. Part of the magnetite was formed on heating in the siltstones of site GE13, as indicated by the higher susceptibility on cooling and the heating/cooling T_c of magnetite. In the samples from sites GE13 and AA, as well as from other sites, a mineral with a T_c around $300-310$°C appears on the cooling curve. This is possibly an iron sulphide created on cooling, after heating to 590 and 700°C, respectively. The white oolithic limestone of GE10 shows large irreversibility above 400°C as a result of newly formed magnetite on heating. This newly formed magnetite possibly oxidizes to hematite when heated to 700°C, as suggested by the low susceptibility of the cooling curve.

Field tests

The reversal test developed by McFadden & McElhinny (1990) and its classification (A, B, C, indeterminate) could be applied to the three sites that recorded normal and reverse polarities: BA, GE18 and BG. The classifications are based on the critical angle γ_c and the angle γ between the means, which is equivalent to using the V_w statistical parameter of Watson (1983). The test is indeterminate for site BA. The resulting classifications C (for site GE18) and B (for site BG) indicate that the ChRM directions have been properly isolated.

The non-parametric fold test of Tauxe & Watson (1994) was carried out on site GE09 and the combined sites GE07 and GE08 based on their proximity and similar age. The individual ChRM directions of site GE09 were corrected for a plunging fold axis. This fold test was positive at the 95% confidence level, as the maximum clustering of the dataset occurs between 81 and 109% unfolding. For sites GE07 and GE08 the fold test is also positive. Maximum clustering occurs between 87 and 104% of unfolding. The positive fold tests show that the recorded remanent magnetizations in sites GE07, GE08 and GE09 are of pre-tilting origin and give confidence in the stability of the palaeomagnetic signal on geological timescales.

Palaeomagnetic results
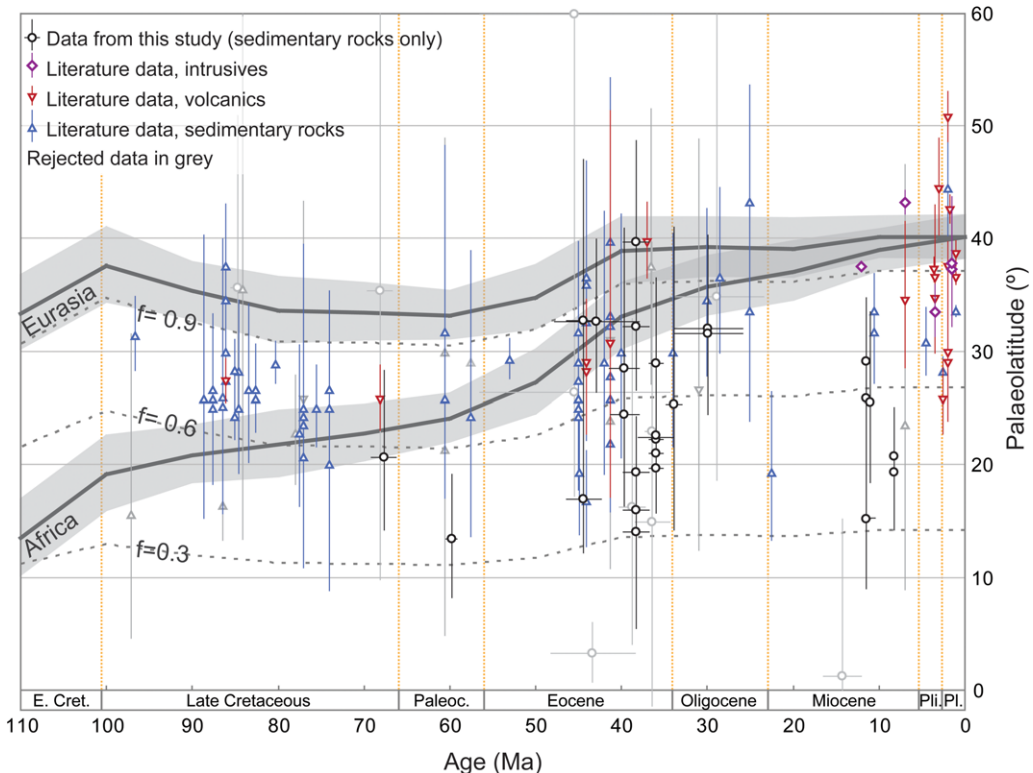
Overall, the retrieval of reliable magnetic records from the Oligocene and Miocene silt/sandstones and mudstones was more difficult than from the Upper Cretaceous, Paleocene and Eocene volcanoclastics and turbidites. This might explain why previous studies concentrated on Upper Cretaceous and Eocene rocks. The site mean directions of the isolated ChRM and secondary magnetization components are listed in Table 1. Among our 37 sites, several give questionable results, which were analysed using a set of reliability criteria. The same reliability criteria were also applied to previously published data.

The calculated palaeolatitudes derived from the palaeomagnetic directions were plotted v. age (Fig. 5). A comparison of the calculated palaeolatitudes with the latitude v. age curves of Eurasia and Africa (Torsvik *et al.* 2012) showed that the great majority

of the accepted sites displayed unrealistically low palaeolatitudes. Possible explanations for the low latitudes are discussed in this paper.

Literature review procedure

The data reviewed in this study consist of all the available sites from the GPMDB in addition to studies published in the English language scientific literature. Data from *c.* 100 sites with Upper Cretaceous to Pleistocene deposits were included in the review. The GPMDB contains results included in later studies that were also entered into the database. To avoid including the same dataset twice, we only included the combined and non-superseded studies in our review. Because we aimed to compare the data and associated errors obtained in this study with those of the database and in the literature, we recalculated the reported α_{95} values in the literature

Fig. 5. Palaeolatitude v. age diagram for the period 110–0 Ma. The Eurasian and African curves (calculated for a reference location in Georgia at $\lambda = 41.3$, $\varphi = 43.7$) with their ΔI_x error (shaded area) are derived from the global apparent polar wander path of Torsvik *et al.* (2012). Black (grey) circles and their error bars show the palaeolatitude and its error (calculated from ΔI_x) for each accepted (rejected) site of this study. Blue triangles/red inverted triangles/purple diamonds and their error bars show the palaeolatitude and its error (calculated from ΔI_x) for each accepted sediment/volcanic/intrusive site of the review data presented in this study. The dotted lines indicate the position of the Eurasian curve calculated with flattening factors (f) of 0.9, 0.6 and 0.3 to show the possible effect of inclination shallowing. Yellow dotted lines subdivide epochs. E. Cret., Early Cretaceous; Paleoc., Paleocene; Pli., Pliocene; Pl., Pleistocene.

to A_{95} values using the Creer transformation (Creer 1962). ΔD_x and ΔI_x were subsequently calculated from the A_{95} values (following Butler 1992).

Reliability criteria
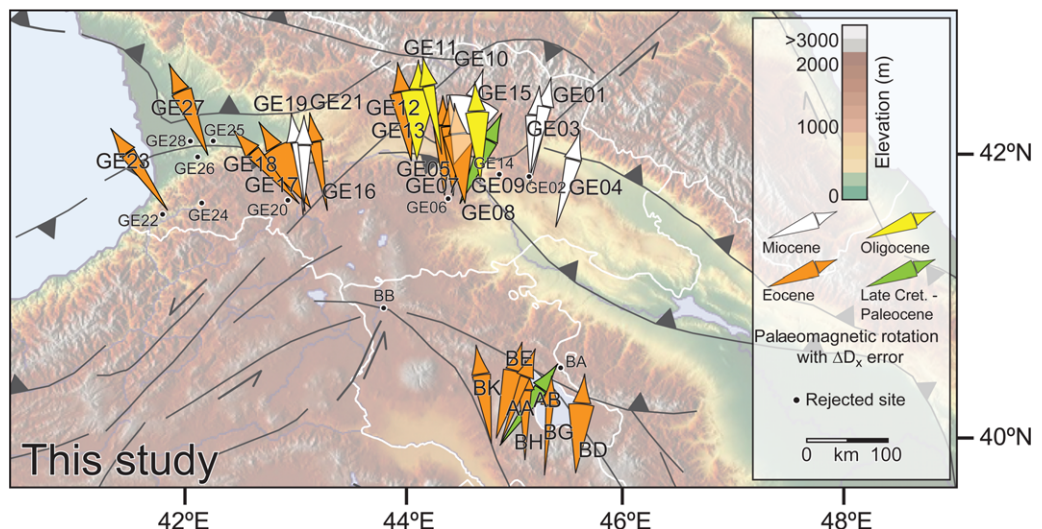
A set of reliability criteria was applied to our data as well as to the literature data presented in this study. However, not all the reliability criteria were applied to the GPMDB data because the available information (e.g. statistics, demagnetization method and tectonic context) was not always sufficient to apply all the reliability criteria. We therefore cannot guarantee that all the GPMDB datasets of low quality (in terms of statistics, demagnetization method and tectonic context) were excluded after applying the reliability criteria. The reliability of this review therefore does not lie in the individual datasets, but in the consistency within the large dataset, i.e. in the spatial and temporal variation of the vertical axis rotations. The reliability criteria listed here were applied to all the data and led to the exclusion of a number of sites (see Table 1).

Sites that did not pass the following criteria were excluded from further analysis.

(1) Sites with less than five samples (N; e.g. sites GE26 and BB) for sediments, or $N<5$ for the number of lava flows sampled (e.g. dataset 158).

(2) Sites with a mean ChRM direction (before tilt correction) that was statistically indistinguishable from the present-day geocentric axial dipole field at the site location ($I = c.\ 60°$; $D = c.\ 0°$). This led to the exclusion of sites GE06, GE14, GE24, GE26, GE28 and BB. Site GE10 was not excluded as a result of the presence of one reversed polarity sample, which gives some confidence that the ChRM could be of primary origin.

(3) Datasets with suspect directions (e.g. north/up or south/down directions), either indicating >90° rotation or deposition in the southern hemisphere (e.g. sites GE06, GE25 and dataset 166).

(4) Datasets that yield an inclination that would have undergone very significant inclination shallowing (flattening factor, $f < 0.3$) or with unrealistically high inclinations (tan $I_{observed} = f$ tan $I_{expected}$; King 1955). The sampled sediments were probably deposited near or on the Eurasian margin and the dotted lines in Figure 5 indicate the position of the Eurasian margin, for the study area, with three different flattening factors ($f = 0.9$, $f = 0.6$ and $f = 0.3$). This criterion led to the rejection of sites GE14 and GE22.

(5) Datasets with an error in declination (ΔD_x) >15° (e.g. sites GE20, BA and dataset 13).

(6) Finally, we removed obvious outliers from the general data trend (see Figs 5 & 6). In the review, these are sites 166 (which was also excluded under criterion 3), 167 and 96 from the Late Cretaceous time slice, as well as site 78 from the Paleocene. These sites have probably been affected by local fault

Fig. 6. Shaded relief digital elevation model of the Caucasus region showing all rotations (calculated following Butler 1992; see text for explanation) with their associated ΔD_x error for the accepted sites from this study. Each colour represents a different age (see legend).

movements or were not recognized as remagnetized sites. The same holds for our site GE20 (sampled in Upper Eocene rocks), which displays a large rotation that is the opposite of all other reported rotations in the area.

Accepted sites after application of the reliability criteria

This study

Nine of the 37 sites were excluded from further analyses based on the listed reliability criteria. The criteria that led to their exclusion are indicated for each site in Table 1. Site GE02 was rejected because no result could be retrieved from the 26 demagnetized specimens.

The finite rotation vectors relative to stable Eurasia are plotted in Figure 6 for the 26 accepted sites presented in this study. The rotation vector (R) was calculated by subtracting the expected declination for stable Eurasia from the observed declination ($R = D_{obs} - D_{exp}$; Butler 1992). The expected declinations have been calculated from the global apparent polar wander path (Torsvik *et al.* 2012) in the Eurasian reference frame at our reference location ($\lambda = 41.3°$N; $\varphi = 43.7°$E). The following corrections (D_{exp}) were applied: $+10°$ for the Late Cretaceous and Paleocene; $+11°$ for the Eocene; $+8.5°$ for the Oligocene; and $+4°$ for the Miocene. Overall the rotations vary from anticlockwise in the western part to slightly clockwise in the eastern part of the orocline, in concordance with earlier findings (Bazhenov & Burtman 2002; Hisarli 2011). The limited geographical spread of the data displayed per time interval does not allow an immediate assessment of the variation in the amount of rotation along the orocline. Our sites sampled from Upper Cretaceous and Paleocene rocks were mostly limited to the eastern part of the study area. The Miocene has only been sampled in the northern part of the orocline because there were no outcrops suitable for sampling in Armenia.

Literature review

The application of the reliability criteria led to the exclusion of 12 sites. Using the same procedure as described in the preceding sections, we calculated the finite rotations for the remaining 88 datasets (following Butler 1992). The number of data in each time slice allowed us to conclude that the rotations not only change from westerly to easterly (from west to east), but also that the amount of rotation is lower in younger than in older rocks. The declinations in the Oligocene, Miocene and Plio-Pleistocene intervals are visibly lower than in the Late Cretaceous and Eocene.

The data from the literature review yielded very low inclinations, especially for the post-Middle Eocene time interval (*c.* 45 Ma and younger; Fig. 5). Possible reasons for the low latitudes are discussed in the following section.

Combined datasets: qualitative observations

A combined examination of Figures 6 and 7 allows the following qualitative observations to be made.

(1) The Late Cretaceous sites (Figs 6 & 7a) show CCW finite rotations in the western part of the Lesser Caucasus. Going eastwards, the rotations evolve progressively to clockwise (CW) rotations.

(2) From Late Cretaceous to Eocene times (Figs 6 & 7a–c), the CW rotations slightly decrease in the eastern limb of the orocline, whereas the rotations are CCW and seemingly of similar amplitude in the central and western parts of the orocline.

(3) In the datasets from Oligocene, Miocene and Pliocene to Pleistocene rocks, generally small (CW as well as CCW) rotations can be observed throughout the study area (Figs 6 & 7d–f). The general trend since the Late Cretaceous therefore shows a decrease in the rotation with time.

Strike test results: a quantitative approach

For the strike tests, we determined a regional strike for each site based on satellite images from the sampling area in combination with geological maps. The regional strikes were assigned a fixed $10°$ uncertainty. The strike tests in Figure 8 are based on linear statistics and the 95% error bands associated with the slopes (m) of the regression lines were calculated following Tukey's range test. We performed the strike test for four time intervals based on the available number of datasets per time interval and the tectonic chronology. The first interval (Late Cretaceous–Paleocene) includes the rocks formed presumably before and during the SAB–Eurasia collision. The datasets from rocks deposited in this time interval (Δt) cover *c.* 40 myr. The second interval covers the Eocene, which represents the time span after initial SAB collision and before the initiation of Arabia–Eurasia collision. Because we have only one dataset from Lower Eocene rocks, all but one dataset in this time interval cover a period of *c.* 12 myr in the Middle and Late Eocene. The third, Oligocene to Pleistocene, interval includes the Arabia–Eurasia collision (Δt *c.* 33 myr). The limited number of available datasets for the Oligocene did not allow us to perform the orocline test for these sites only. We do, however,

present a separate orocline test for data from Late Miocene to Pleistocene rocks. The time interval for this test is therefore limited to c. 12 myr.

The Late Cretaceous to Paleocene strike test (Fig. 8a) gave a slope $m = 0.604 \pm 0.255$ (correlation coefficient, $R^2 = 0.395$). The result shows that (within 95% confidence limits) some pre-Late Cretaceous curvature must have existed because $m < 1$. We performed two different tests for the Eocene period (Fig. 8b): one with all accepted data ($m = 0.324 \pm 0.147$, $R^2 = 0.328$) and a second test that excluded five points ($m = 0.479 \pm 0.133$, $R^2 = 0.608$) that were obvious outliers (Figs 6 & 7c). The latter test resulted in a better fit and much higher R^2 value. For both Eocene tests, the slope (m) is lower than for the Late Cretaceous to Paleocene strike test. Both results are, however, not statistically distinguishable within the 95% confidence limits from the Late Cretaceous to Paleocene strike test. The Oligocene to Pleistocene strike test (Fig. 8c; $m = -0.092 \pm 0.163$, $R^2 = 0.032$) results in a slope that is indistinguishable from $m = 0$. We note, however, that the number of datasets from Oligocene rocks is limited and the Oligocene to Pleistocene strike test covers a very long time interval (c. 33 myr). We therefore performed a strike test on all the data from Upper Miocene to Pleistocene rocks (Fig. 8d), which represents only a c. 12 myr time slice. The Late Miocene to Pleistocene strike test results in $m = -0.078 \pm 0.187$ and $R^2 = 0.023$.

Discussion

Oroclinal bending

The results from the strike tests indicate that the Eastern Pontides–Lesser Caucasus orocline falls within the field of progressive oroclines (Fig. 3; Weil & Sussman 2004; Johnston et al. 2013). Some pre-existing Late Cretaceous curvature (c. $40 \pm 25\%$) must have been present because the slope of the Late Cretaceous to Paleocene strike test is significantly less than unity. The slopes of the two strike tests performed on data from Eocene rocks are slightly less steep than for the Late Cretaceous to Paleocene, indicating that orocline formation probably initiated before the Eocene as a result of SAB–Eurasia collision. The results are, however, not statistically distinguishable for the two time intervals. Our preferred Eocene strike test, which excludes five outliers, indicates that c. $48 \pm 13\%$ of orocline formation occurred after the Eocene. The Oligocene to Pleistocene strike test, with a slope that was statistically indistinguishable from zero, seems to indicate that orocline formation occurred entirely before the Oligocene. However, the number of data entries for the Oligocene is
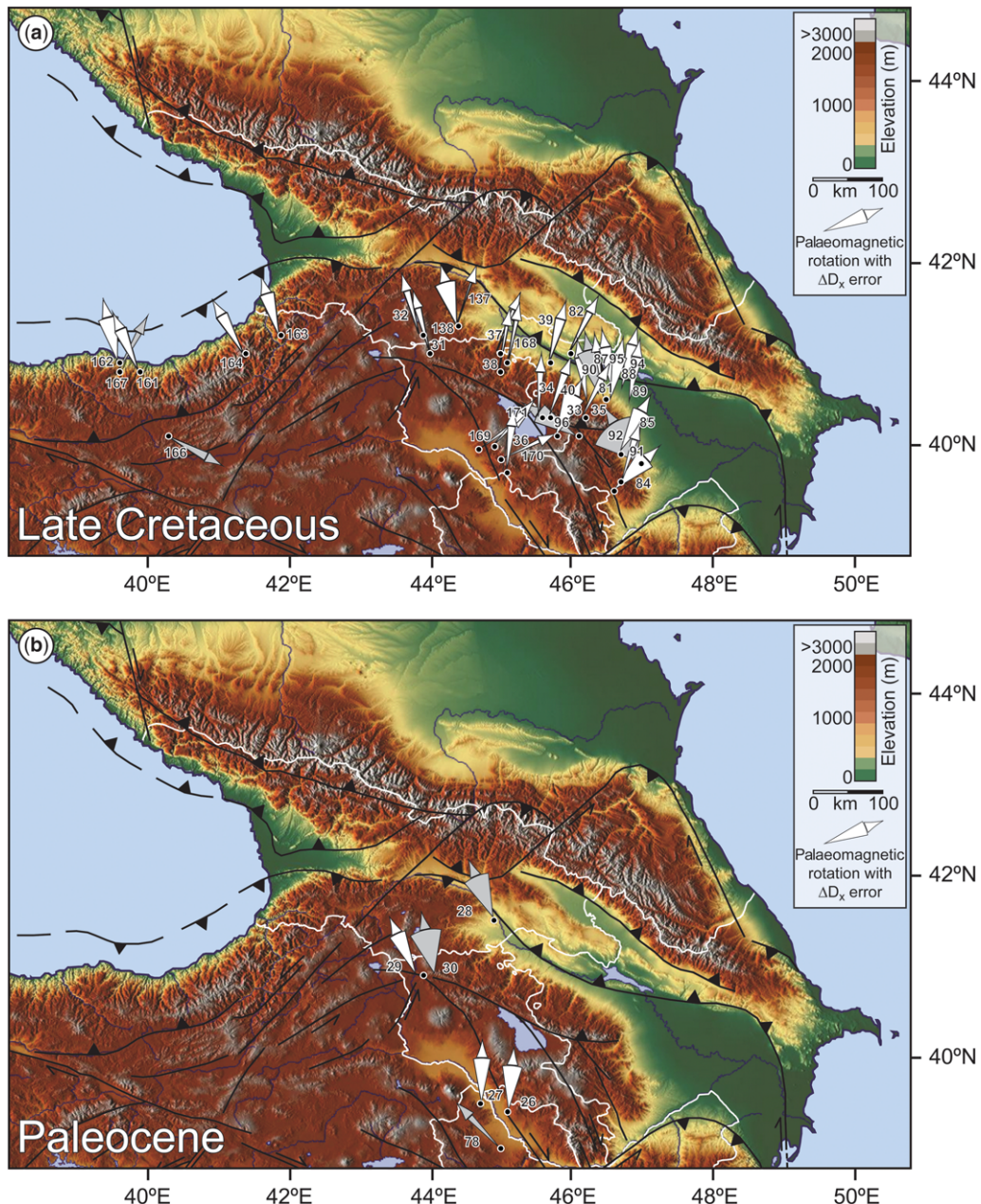
limited ($N = 8$), the data are very scattered and the sites are not homogenously distributed over the study area (Figs 6 & 7d and open circles in Fig. 8c). Therefore we conclude that the data from Oligocene rocks do not allow us to constrain the timing of orocline formation. The strike test for the Late Miocene to Pleistocene interval (Δt c. 12 myr) results in a slope that is statistically indistinguishable from zero. We note, however, that the regression line is poorly defined (Fig. 8d). We thus conclude that orocline formation probably ended before the Late Miocene. A study of pre-Late Cretaceous rocks is necessary to determine whether the pre-existing Late Cretaceous curvature resulted from oroclinal bending or whether this curvature is an inherited physiographical feature (i.e. a primary orogenic bend; see Fig. 3).

Despite some limitations in the number of datasets – per time interval, as well as in terms of geographical spread – a coherent chronological trend emerges from the strike test (Fig. 8). We argue that about 40% of the curvature of the Eastern Pontides–Lesser Caucasus fold–thrust belt was acquired before the Late Cretaceous and c. 60% between the Paleocene and probably the Late Miocene. Even though the Late Cretaceous–Paleocene and Eocene strike tests (Fig. 8a, b) result in slopes that are statistically indistinguishable from each other, these two tests suggest that c. 10% of the curvature was acquired after the Paleocene and before the Middle Eocene, most probably as a consequence of SAB–Eurasia collision. The remaining c. 50% (Fig. 8b, excluding outliers) occurred after the Late Eocene and probably before the Late Miocene (Fig. 8d) and therefore includes the time interval of Arabia–Eurasia collision. Consequently, we conclude that c. 50% of the belt's curvature developed in response to Arabia–Eurasia collision. The interpretation of the strike tests of the present study is slightly different from that given by Bazhenov & Burtman (2002) and Hisarli (2011). All three studies agree that the curvature of the belt developed mostly after the Late Cretaceous to Eocene, but Bazhenov & Burtman (2002) and Hisarli (2011) did not conclude that the belt had an existing curvature before the Late Cretaceous to Paleocene. The slopes of the regression lines presented by Hisarli (2011) after the removal of several outliers are, however, slightly lower than unity and lower for the Eocene than for the Late Cretaceous, suggesting progressive oroclinal bending as in our study. We stress that the main difference between this study and the two earlier studies is that we performed a more rigorous strike test on a much larger number of data (including the data from both earlier publications).

After the Eocene, the ongoing convergence and collision between Arabia and Eurasia led to the

exhumation of the western Greater Caucasus (Vincent *et al.* 2007) – which has rapidly accelerated since the earliest Pliocene in the central Greater Caucasus (Avdeev & Niemi 2011) – and exhumation in the Bitlis–Zagros thrust zone in the Early to Middle Miocene (Okay *et al.* 2010). Over


Fig. 7. Shaded relief digital elevation models of the Caucasus region showing all rotations (calculated following Butler 1992; see text for explanation) with their associated ΔD_x error for the accepted (white) and rejected (grey) sites from the presented review for the (**a**) Late Cretaceous, (**b**) Paleocene, (**c**) Eocene, (**d**) Oligocene, (**e**) Miocene and (**f**) Plio-Pleistocene. Numbers refer to the numbers that were assigned to each study in Supplementary Data Table 2.
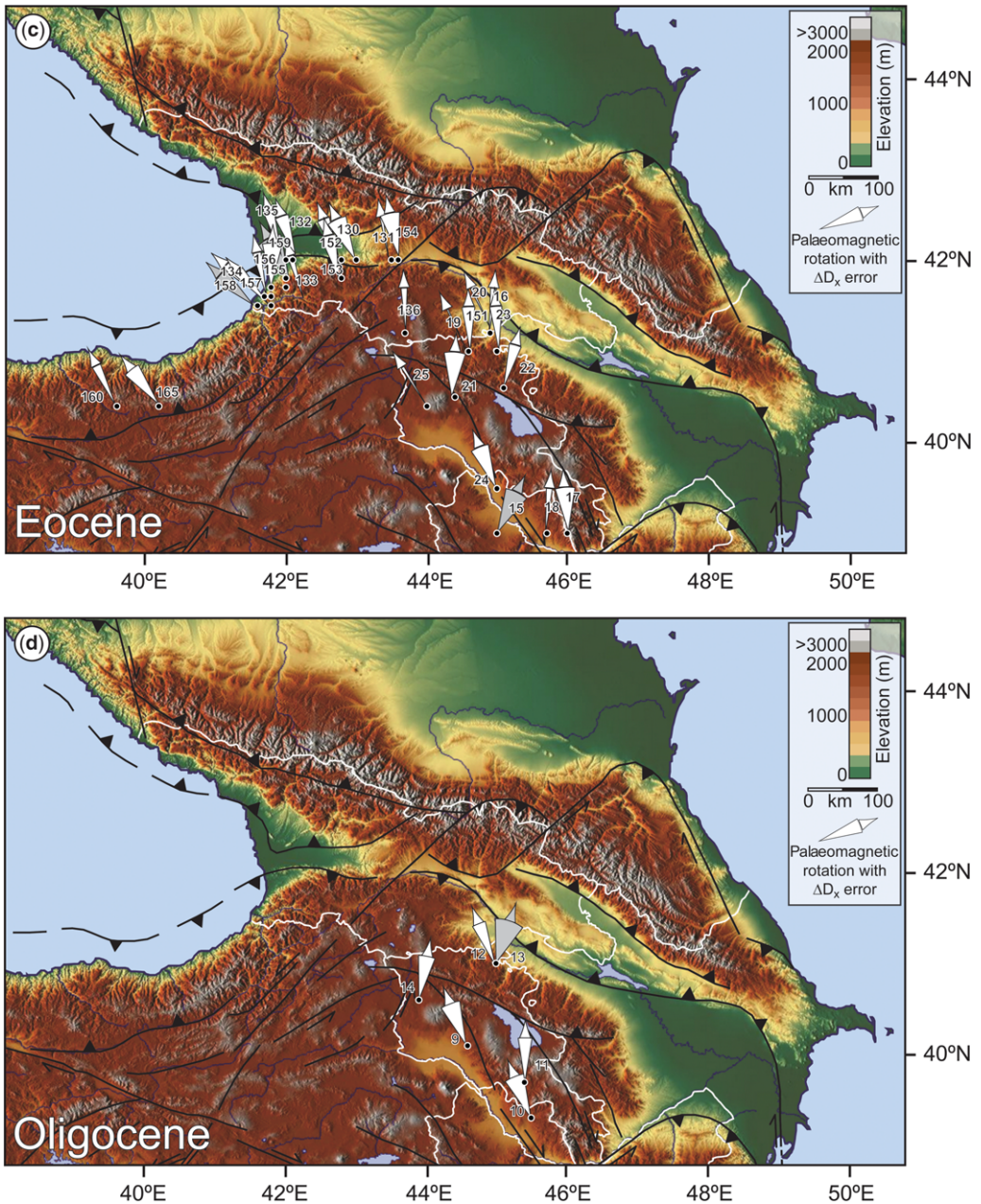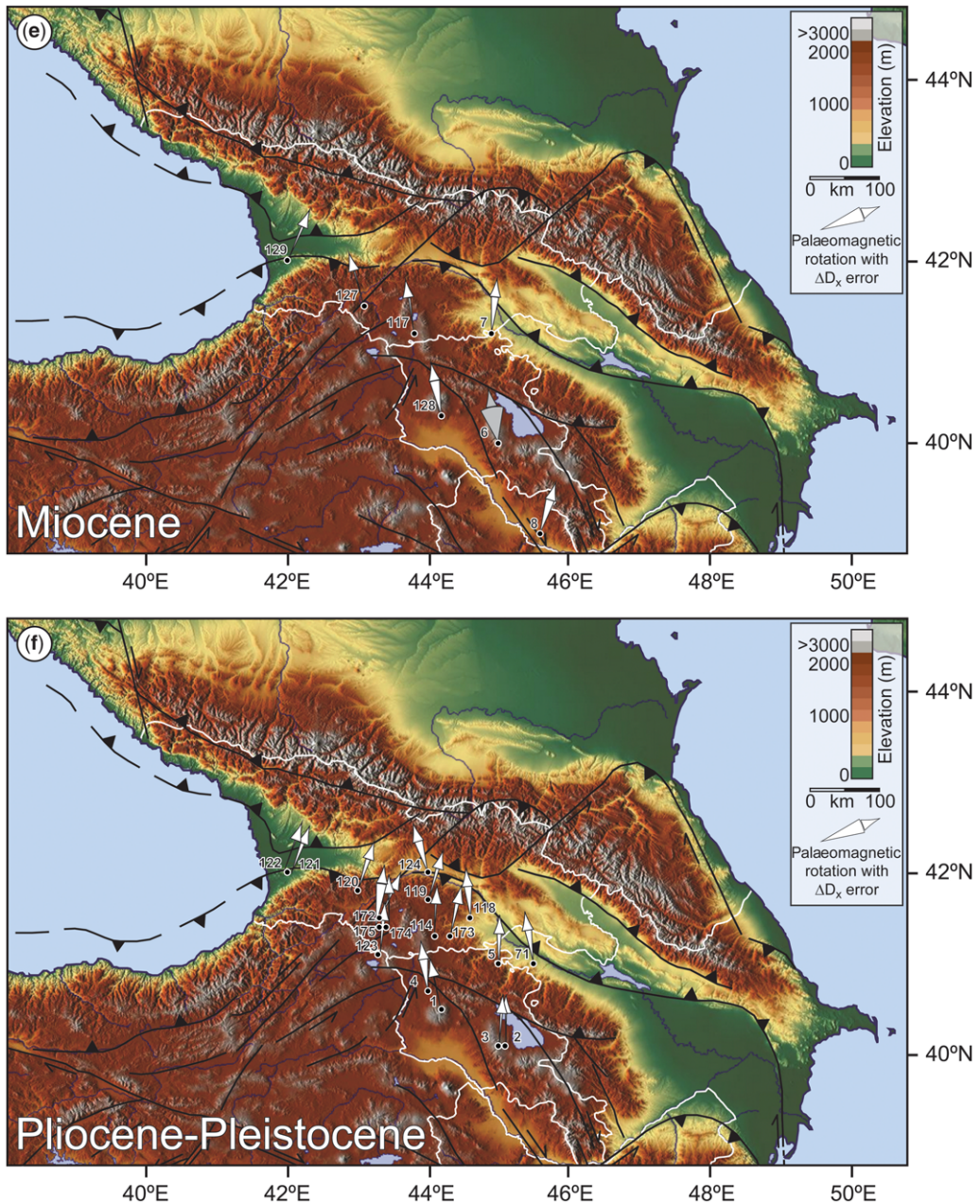
Fig. 7. *Continued.*

the last few million years, the region has been characterized by localized deformation, as evidenced by the significant amount of shortening in a narrow zone between the Greater and Lesser Caucasus (Forte *et al.* 2013), as well as by Anatolian escape tectonics since the Late Miocene (Dewey & Şengör 1979; Şengör *et al.* 1985). Oroclinal bending most probably ended before the Late Miocene and therefore potentially predates the transformation of distributed to more localized deformation in the region. The entire Lesser Caucasus region continued to experience deformation
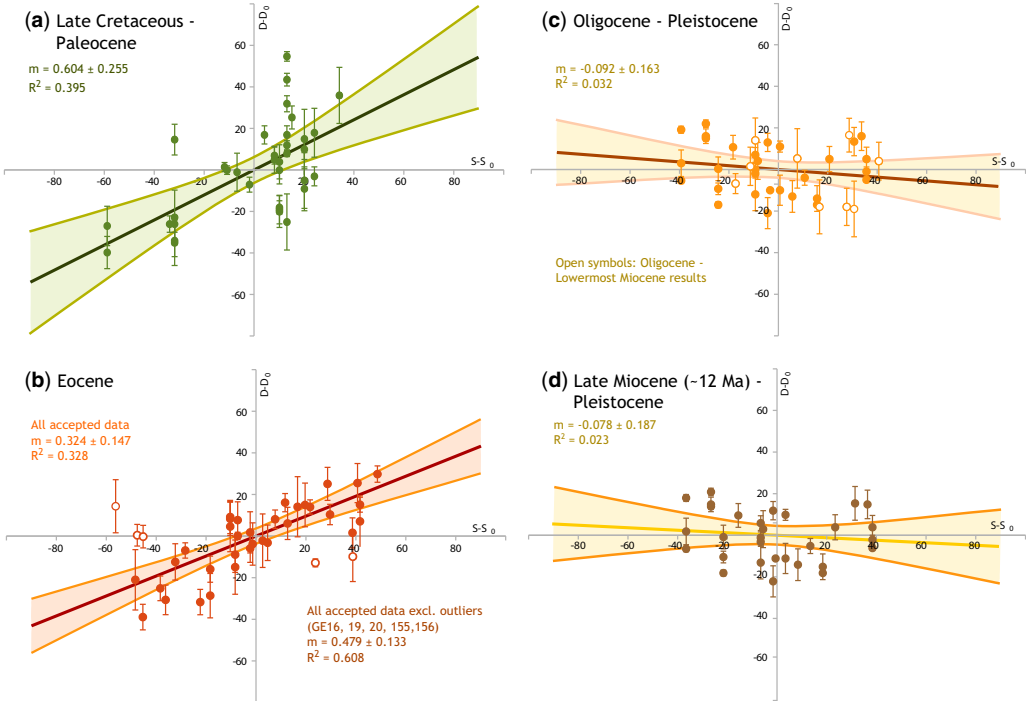
Fig. 7. *Continued.*

after the Late Miocene, as shown by Copley and Jackson (2006), who investigated how active faulting accommodates Arabia–Eurasia collision in the Turkish–Iranian Plateau. Copley and Jackson (2006) proposed a model of CCW rotating blocks bounded by right-lateral strike-slip faults in the central part of the Lesser Caucasus. This is consistent with the overall CCW rotation of the Lesser Caucasus region as shown by geodetic displacement vectors (Reilinger *et al.* 2006; Kadirov *et al.* 2008; Djamour *et al.* 2011; Karakhanyan *et al.* 2013).

Fig. 8. Palaeomagnetic strike tests for data from the Lesser Caucasus orocline for (**a**) Upper Cretaceous to Paleocene rocks, (**b**) Eocene rocks, (**c**) Oligocene to Pleistocene rocks (including Oligocene and Neogene rocks and (**d**) Upper Miocene to Pleistocene rocks. Best-fit slopes through the datasets and their 95% confidence estimates are plotted for each individual strike test. m, slope of the regression line; R^2, correlation coefficient; D, actual declination; D_0, reference declination (in this paper the average declination of the dataset); S, actual strike; S_0 = reference strike (in this paper, the average strike in the area around the dataset). See text for further details.

The timing of orocline formation in the Eastern Pontides–Lesser Caucasus is not coeval with orocline formation in the Central Pontides and Central Alborz Mountains. In the Central Pontides, orocline formation occurred in the latest Cretaceous or Paleocene in response to collision of the Central Anatolian Crystalline Complex with Eurasia (Fig. 1a; Meijers *et al.* 2010; Lefebvre *et al.* 2013) and had ended by the Eocene. It therefore predated orocline formation in the Lesser Caucasus region. In contrast, oroclinal bending in the Central Alborz Mountains occurred after *c.* 7.6 Ma (Late Miocene), possibly as a result of the relative motion between rigid crustal blocks in the collision zone (Cifelli *et al.* 2015), therefore post-dating orocline formation in the Eastern Pontides–Lesser Caucasus belt. Although oroclinal bending in the Eastern Pontides–Lesser Caucasus seems to have been a process that went on for more than 70 myr, oroclinal bending in the Central Alborz Mountains and the Central Pontides was of much shorter duration.

The results of the strike tests are highly influenced by the assigned regional strike for each individual site, based on satellite images in combination with geological maps. Therefore we emphasize that detailed structural mapping of the area surrounding each site would probably improve the accuracy of our strike tests and allow a better comparison between our results and the proposed tectonic models for the region. Detailed structural mapping around all our sampling locations, as well as around the sites from the literature review, was, however, beyond the scope of this study.

Low palaeolatitudes

All the sampled rocks from this study and the literature data were deposited on the Eurasian margin or close to the Eurasian margin (the sites sampled in the SAB; Meijers *et al.* 2015). All the presented datasets should therefore plot within error above the African or below the Eurasian palaeolatitude v. age curve of Figure 5. The estimated shortening within the fold–thrust belt and unbending of the Lesser Caucasus orocline must be taken into account, however, which was estimated to be

>400 km by Bazhenov & Burtman (2002). The correction for this shortening, which occurred mostly in a north–south direction, positions the Eurasian margin *c*. 4° further south (given that 110 km corresponds to *c*. 1° in latitude) and thus reduces the palaeolatitudinal gap. The palaeolatitudes in the compilation in this study are often more than 4° lower than the calculated palaeolatitudes from the apparent polar wander path (Fig. 5) and can therefore only partially be explained by shortening in the Caucasus region between stable Eurasia and Arabia. We therefore explore the possibility of other processes that could result in low inclinations.

The calculated palaeolatitudes (Fig. 5) underscore three main points.

(1) The data distribution is heterogeneous (e.g. there are a sizeable number of datasets for the Middle to Late Eocene, but not for the Early Eocene, very few data for the Oligocene and almost no data for the Early and Middle Miocene).

(2) The palaeolatitude scatter for some time intervals is considerable (e.g. for the Middle and Late Eocene).

(3) The palaeolatitudes are often much lower than expected for the Middle to Late Eocene and the Late Miocene to Pleistocene.

The only time interval for which nearly all results display the expected palaeolatitudes is the Upper Cretaceous (*c*. 100–60 Ma). Many datasets in the 100–60 Ma interval plot between the African and Eurasian curve and are statistically indistinguishable from the Eurasian curve.

One of the possible causes for low palaeolatitudes is a bias in the recording of the remanence by the rock itself, in particular inclination shallowing, which only affects sedimentary rocks. Inclination shallowing is a (post-)depositional process in sedimentary rocks that can lead to an underestimation of the palaeolatitude. Typical flattening factors (*f*) range from 0.4 to 0.83 for hematite-bearing rocks and from 0.54 to 0.79 for magnetite-bearing rocks (Bilardello & Kodama 2010). To test for inclination shallowing, we subdivided all the data into three groups: datasets from: (1) sedimentary rocks (64 accepted sites; including all sites from this study); (2) extrusive volcanic rocks (19 accepted sites); and (3) intrusive rocks (five accepted sites; Fig. 5). Whenever a site consisted of a combination of volcanic and sedimentary rocks it was labelled as sedimentary rock. We distinguished between extrusive volcanic and intrusive rocks because, even though intrusive bodies are unlikely to experience significant post-emplacement tilting, they cannot be corrected for tilting. The subdivision of the data in the three groups shows that the volcanic rocks (in red, Fig. 5) yielded expected inclinations for Eocene

and older rocks, unlike the sedimentary rocks that mostly displayed palaeolatitudes that were too low from *c*. 60 Ma to recent. A portion of the Pliocene to Pleistocene magmatic (extrusive volcanics + intrusives) rocks displays low as well as relatively high palaeolatitudes.

Inclination shallowing can thus be a possible explanation for the low latitudes of sedimentary rocks younger than *c*. 60 Ma, but not for the low ($N = 5$) and high ($N = 1$) palaeolatitudes observed in Pliocene to Pleistocene recent magmatic rocks. We note that the lowest palaeolatitudes in these magmatic rocks come from old datasets and are possibly caused by an error in the determination of the ChRM direction. We must keep in mind, however, that often no information is provided on the demagnetization procedure or on the bedding tilt corrections performed on the sites from the literature data, even though the datasets passed our reliability criteria. In addition, insufficient averaging of secular variation for the intrusive and volcanic rocks and unrecognized remagnetizations (for the literature data) could be a cause for palaeolatitudes that deviate from the Eurasian curve. Not averaging the secular variation of the Earth's magnetic field can lead to a direction that represents an instantaneous field direction instead of that of the geocentric axial dipole hypothesis. Palaeolatitude errors related to the latter possibility would not be biased towards low palaeolatitudes and could therefore explain the spread between too low as well as too high palaeolatitudes in the data from the magmatic rocks for the Pliocene to Pleistocene time interval.

A last possible explanation for the low palaeolatitudes is the contribution of a significant octupolar field to the mostly dipolar Earth's magnetic field. This hypothesis has been proposed by several researchers for the inclination shallowing observed in Cenozoic rocks from Central Asia (Si & Van der Voo 2001; Dupont-Nivet *et al.* 2010), although it has been disproved by others (Camps & Prévot 1996; Camps *et al.* 2007). The effect of an octupolar contribution to the Earth's magnetic field that would influence the inclination in the Lesser Caucasus region would, however, affect all datasets similarly, disregarding the sampled rock types. The large scatter of palaeolatitudes between *c*. 45 and *c*. 30 Ma rules out this hypothesis; differential shallowing of the inclination (depending on the lithology of the sampled rocks) is a more viable explanation for the spread in palaeolatitudes.

A correction for *c*. 4° of shortening within the Caucasus region (for the Eocene and, to a lesser degree, for younger rocks), variable amounts of inclination shallowing in the sedimentary rocks and insufficient averaging of secular variation in the Pliocene to Pleistocene volcanic rocks can explain

the majority of the low inclination data of Eocene and younger rocks in Figure 5. Inclination shallowing would, however, not or hardly affect the declination, whereas insufficient averaging of secular variation would result in erroneous declinations.

Conclusions

Our newly presented palaeomagnetic data, supplemented with published data from Upper Cretaceous to Pleistocene rocks, allow us to confirm that the Eastern Pontides–Lesser Caucasus fold–thrust belt is a progressive orocline. To date oroclinal bending and relate it to tectonic events, a strike test was performed on four intervals that were subdivided based on tectonic chronology: (1) the Late Cretaceous–Paleocene, a period that includes the rocks formed during SAB–Eurasia collision; (2) the Eocene, representing the time span between ongoing SAB–Eurasia collision and the initiation of Arabia–Eurasia collision; (3) the Oligocene to Pleistocene, a time span that includes Arabia–Eurasia collision; and (4) the Late Miocene to Pleistocene. The strike test shows that c. 40% of the arcuate shape was acquired before the Late Cretaceous and c. 60% after the Late Cretaceous to Paleocene time period. The pre-Late Cretaceous curvature could have been a pre-exiting physiographical feature or formed by oroclinal bending due to an earlier tectonic event. Possibly c. 10% of the curvature developed between the Paleocene and the Middle Eocene as a result of SAB–Eurasia collision. The remaining c. 50% of curvature occurred after the Late Eocene and before the Late Miocene, most probably as a consequence of Arabia–Eurasia collision.

The palaeolatitudes calculated from the palaeomagnetic data are generally low in the c. 45 Ma to present time interval. These low palaeolatitudes are probably caused by a combination of factors: (1) shortening within the fold–thrust belt north of the orocline; (2) inclination shallowing (for sediments only); and/or (3) an under-sampling of palaeo-secular variation in Pliocene to Pleistocene volcanic rocks from older studies.

References

ADAMIA, SH., ZAKARIADZE, G., CHKHOTUA, T., SADRADZE, N., TSERETELI, N., CHABUKIANI, A. & GVENTSADZE, A. 2011. Geology of the Caucasus: a review. *Turkish Journal of Earth Sciences*, **20**, 489–544. http://doi.org/10.3906/yer-1005-11

AGARD, P., OMRANI, J. ET AL. 2011. Zagros orogeny: a subduction-dominated process. *Geological Magazine*, **148**, 692–725.

AGHAMALYAN, V. A. 1998. The basement crystalline of Armenia. PhD dissertation, Institute of Geological Sciences, National Academy of Sciences of Armenia [in Russian].

ALLEN, M., JACKSON, J. A. & WALKER, R. 2004. Late Cenozoic reorganization of the Arabia–Eurasia collision and the comparison of short-term and long-term deformation rates. *Tectonics*, **23**. http://doi.org/10.1029/2003TC001530

ALLEN, M. B. & ARMSTRONG, H. A. 2008. Arabia–Eurasia collision and the forcing of mid-Cenozoic global cooling. *Palaeogeography, Palaeoclimatology, Palaeoecology*, **265**, 52–58.

ALLEN, M. B., VINCENT, S. J., ALSOP, G. I., ISMAIL-ZADEH, A. & FLECKER, R. 2003. Late Cenozoic deformation in the South Caspian region: effects of a rigid basement block within a collision zone. *Tectonophysics*, **366**, 223–239.

ASATRYAN, G., DANELIAN, T. ET AL. 2012. Radiolarian biostratigraphic constraints for latest Jurassic-earliest Cretaceous submarine volcanic activity in the Tethyan oceanic realm of the Sevan ophiolite (Armenia). *Bulletin de la Société géologique de France*, **183**, 319–330.

AVAGYAN, A., SOSSON, M. ET AL. 2005. Neogene to Quaternary stress field evolution in Lesser Caucasus and adjacent regions using fault kinematics analysis and volcanic cluster data. *Geodinamica Acta*, **18**, 401–416.

AVAGYAN, A., SOSSON, M. ET AL. 2010. Recent tectonic stress evolution in the Lesser Caucasus and adjacent regions. *In*: SOSSON, M., KAYMAKCI, N., STEPHENSON, R. A., BERGERAT, F. & STAROSTENKO, V. (eds) *Sedimentary Basin Tectonics from the Black Sea and Caucasus to the Arabian Platform*. Geological Society, London, Special Publications, **340**. 393–408. http://doi.org/10.1144/SP340.17

AVDEEV, B. & NIEMI, N. 2011. Rapid Pliocene exhumation of the central Greater Caucasus constrained by low-temperature thermochronometry. *Tectonics*, **30**, TC2009. http://doi.org/10.1029/2010TC002808

AXEN, G. J., LAM, P. S., GROVE, M., STOKLI, D. F. & HASSANZADEH, J. 2001. Exhumation of the west-central Alborz mountain, Iran, Caspian subsidence, and collision-related tectonics. *Geology*, **29**, 559–562. http://doi.org/10.1130/0091-7613(2001)029<0559:EOTWCA>2.0.CO;2

BALLATO, P., UBA, C. E. ET AL. 2011. Arabia-Eurasia continental collision: insights from late Tertiary

foreland-basin evolution in the Alborz mountains, northern Iran. *Geological Society of America Bulletin*, **123**, 106–131.

BAZHENOV, M. L. & BURTMAN, V. S. 2002. Eocene paleomagnetism of the Caucasus (southwest Georgia): oroclinal bending in the Arabian syntaxis. *Tectonophysics*, **344**, 247–259.

BELOV, A. A. & SOKOLOV, S. D. 1973. Relics of Mesozoic oceanic crust among the crystalline complexes of the Miskhana massif of Armenia. *Sovetskaya Geologia*, **8**, 26–41 [in Russian].

BELOV, A. A., BRAGIN, N. Yu., VISHNEVSKAYA, V. S., SATIAN, M. & SOKOLOV, S. D. 1991. *New Data About the Age of the Ophiolites of Vedi (Armenia)*. Reports of the USSR Academy of Science **321**, 784–787 [in Russian].

BERBERIAN, M. & KING, G. C. P. 1981. Towards a paleogeography and tectonic evolution of Iran. *Journal Canadien des Sciences de la Terre (Canadian Journal of Earth Sciences)*, **18**, 210–265.

BILARDELLO, D. & KODAMA, K. P. 2010. Rock magnetic evidence for inclination shallowing in the early Carboniferous Deer Lake Group red beds of western Newfoundland. *Geophysical Journal International*, **181**, 275–289. http://doi.org/10.1111/j.1365-246X.2010.04537.x

BUTLER, R. F. (eds) 1992. *Paleomagnetism: Magnetic Domains to Geologic Terranes*. Blackwell Scientific, Boston.

CAMPS, P. & PRÉVOT, M. 1996. A statistical model of the fluctuations in the geomagnetic field from paleosecular variation to reversal. *Science*, **273**, 776–779.

CAMPS, P., HENRY, B., NICOLAYSEN, K. & PLENIER, G. 2007. Statistical properties of paleomagnetic directions in Kerguelen lava flows: implication for the Late Oligocene paleomagnetic field. *Journal of Geophysical Research*, **112**, B06102. http://doi.org/10.1029/2006JB004648

CAREY, S. W. 1955. The orocline concept in geotectonics. *Proceedings of the Royal Society of Tasmania*, **89**, 255–288.

CIFELLI, F., BALLATO, P., ALIMOHAMMADIAN, H., SABOURI, J. & MATTEI, M. 2015. Tectonic magnetic lineation and oroclinal bending of the Alborz range: implications on the Iran-Southern Caspian geodynamics. *Tectonics*, **34**, 116–132. http://doi.org/10.1002/2014TC003626

COPLEY, A. & JACKSON, J. 2006. Active tectonics of the Turkish-Iranian Plateau. *Tectonics*, **25**, TC6006, http://doi.org/10.1029/2005TC001906

CREER, K. M. 1962. The dispersion of the geomagnetic field due to secular variation and its determination for remote times from paleomagnetic data. *Journal of Geophysical Research*, **67**, 3461–3476.

CREER, K. M., IRVING, E. & NAIRN, A. E. M. 1959. Paleomagnetism of the Great Whin Sill. *Geophysical Journal of the Royal Astronomical Society*, **2**, 306–323.

DANELIAN, T., ASATRYAN, G., SOSSON, M., PERSON, A., SAHAKYAN, L. & GALOYAN, G. 2008. Discovery of two distinct Middle Jurassic Radiolarian assemblages in the sedimentary cover of the Vedi ophiolite (Lesser Caucasus, Armenia). *Comptes Rendus Palevol*, **7**, 324–334.

DANELIAN, T., ASATRYAN, G., SAHAKYAN, L., GALOYAN, G., SOSSON, M. & AVAGYAN, A. 2010. New and revised Radiolarian biochronology for the sedimentary cover of ophiolites in the Lesser Caucasus (Armenia). *In*: SOSSON, M., KAYMAKCI, N., STEPHENSON, R. A., BERGERAT, F. & STAROSTENKO, V. (eds) *Sedimentary Basin Tectonics from the Black Sea and the Caucasus to the Arabian Platform*. Geological Society, London, Special Publications, **340**, 383–391. http://doi.org/10.1144/SP340.16

DANELIAN, T., ASATRYAN, G., GALOYAN, G., SOSSON, M., SAHAKYAN, L., CARIDROIT, M. & AVAGYAN, A. 2012. Geological history of ophiolites in the Lesser Caucasus and correlation with the Izmir-Ankara-Erzincan suture zone: insights from radiolarian biochronology. *Bulletin de la Société Géologique de France*, **183**, 331–342.

DEENEN, M. H. L., LANGEREIS, C. G., VAN HINSBERGEN, D. J. J. & BIGGIN, A. J. 2011. Geomagnetic secular variation and the statistics of palaeomagnetic directions. *Geophysical Journal International*, **186**, 509–520.

DEWEY, J. F. & ŞENGÖR, A. M. C. 1979. Aegean and surrounding regions: complex multiplate and continuum tectonics in a convergent zone. *Geological Society of America Bulletin*, **90**, 84–92.

DJAMOUR, Y., VERNANT, P. *ET AL.* 2010. GPS and gravity constraints on continental deformation in the Alborz mountain range, Iran. *Geophysical Journal International*, **183**, 1287–1301. http://doi.org/10.1111/j.1365-246X.2010.04811.x

DJAMOUR, Y., VERNANT, P., NANKALI, H. R. & TAVAKOLI, F. 2011. NW Iran-eastern Turkey present-day kinematics: results from the Iranian permanent GPS network. *Earth and Planetary Science Letters*, **307**, 27–34. http://doi.org/10.1016/j.epsl.2011.04.029

DUPONT-NIVET, G., VAN HINSBERGEN, D. J. J. & TORSVIK, T. H. 2010. Persistently low Asian paleolatitudes: implications for the India-Asia collision history. *Tectonics*, **29**, TC5016.

ELDREDGE, S., BACHTADSE, V. & VAN DER VOO, R. 1985. Paleomagnetism and the orocline hypothesis. *Tectonophysics*, **119**, 153–179.

FORTE, A. M., COWGILL, E., BERNARDIN, T., KREYLOS, O. & HAMANN, B. 2010. Late Cenozoic deformation of the Kura fold-thrust belt, southern Greater Caucasus. *Geological Society of America Bulletin*, **122**, 465–486.

FORTE, A. M., COWGILL, E., MURTUZAYEV, I., KANGARLI, T. & STOICA, M. 2013. Structural geometries and magnitude of shortening in the eastern Kura fold-thrust belt, Azerbaijan: implications for the development of the Greater Caucasus Mountains. *Tectonics*, **32**, 688–717. http://doi.org/10.1002/tect.20032

GALOYAN, G. 2008. *Etudes pétrologiques, géochimiques et géochronologiques des ophiolites du Petit Caucase (Arménie)*, PhD thesis, University of Nice-Sophia Antipolis [in French].

GALOYAN, G., ROLLAND, Y., SOSSON, M., CORSINI, M. & MELKONIAN, R. 2007. Evidence for superposed MORB, oceanic plateau and volcanic arc series in the Lesser Caucasus (Stepanavan, Armenia). *Comptes Rendus Geosciences*, **339**, 482–492.

GALOYAN, G., ROLLAND, Y., SOSSON, M., CORSINI, M., BILLO, S., VERATI, C. & MELKONYAN, R. 2009.

Geology, geochemistry and $^{40}Ar/^{39}Ar$ dating of Sevan ophiolites (Lesser Caucasus, Armenia): evidence for Jurassic back-arc opening and hot spot event between the South Armenian Block and Eurasia. *Journal of Asian Earth Sciences*, **34**, 135–153.

GUEST, B., HORTON, B. K., AXEN, G. J., HASSANZADEH, J. & MCINTOSH, W. C. 2007. Middle to late Cenozoic basin evolution in the western Alborz Mountains: implications for the onset of collisional deformation in northern Iran. *Tectonics*, **26**, TC6011. http://doi.org/10.1029/2006TC002091

HÄSSIG, M., ROLLAND, Y., SOSSON, M., GALOYAN, G., MÜLLER, C., AVAGYAN, A. & SAHAKYAN, L. 2013. Geology and structure of the Amasia ophiolites, NW Sevan-Akera suture zone, Lesser Caucasus, insights for a large-scale obduction in Armenia and NE Turkey. *Tectonophysics*, **588**, 135–153. http://doi.org/10.1016/j.tecto.2012.12.003

HÄSSIG, M., ROLLAND, Y. *ET AL.* 2014*a*. Linking the NE Anatolian and Lesser Caucasus ophiolites: evidence for large-scale obduction of oceanic crust and implications for the formation of the Lesser Caucasus-Pontides Arc. *Geodinamica Acta*. http://doi.org/10.1080/09853111.2013.877236.

HÄSSIG, M., ROLLAND, Y. *ET AL.* 2014*b*. Multi-stage metamorphism in the South Armenian Block during the Late Jurassic to Early Cretaceous: tectonics over south-dipping subduction of Northern branch of Neotethys. *Journal of Asian Earth Sciences*, **102**, 4–23. http://doi.org/10.1016/j.jseaes.2014.07.018

HISARLI, Z. M. 2011. New paleomagnetic constraints on the late Cretaceous and early Cenozoic tectonic history of the Eastern Pontides. *Journal of Geodynamics*, **52**, 114–128, http://doi.org/10.1016/j.jog.2010.12.004

JACKSON, J. 1992. Partitioning of strike-slip convergent motion between Eurasia and Arabia in eastern Turkey and the Caucasus. *Journal of Geophysical Research*, **97**, 12471–12479.

JOHNSTON, S. T., WEIL, A. B. & GUTIÉRREZ-ALONSO, G. 2013. Oroclines: thick and thin. *GSA Bulletin*, **125**, 643–663. http://doi.org/10.1130/B30765.1

KADIROV, F., MAMMADOV, S., REILINGER, R. & MCCLUSKY, S. 2008. Some new data on modern tectonic deformation and active faulting in Azerbaijan (according to Global Positioning System measurements). *The Sciences of the Earth, Proceedings of the Azerbaijan National Academy of Sciences*, **1**, 82–88.

KARAKHANYAN, A., VERNANT, P. *ET AL.* 2013. GPS constraints on the continental deformation in the Armenian region and Lesser Caucasus. *Tectonophysics*, **592**, 39–45.

KARYAKIN, Y. V. 1989. *Geodynamics of the Formation of the Volcanic Complexes of the Lesser Caucasus*. Nauka, Moscow [in Russian].

KAZMIN, V. G., SBORTSHIKOV, I. M., RICOU, L.-E., ZONENSHAIN, L. P., BOULIN, J. & KNIPPER, A. L. 1986. Volcanic belts as markers of the Mesozoic-Cenozoic active margin of Eurasia. *Tectonophysics*, **123**, 123–152. http://doi.org/10.1016/0040-1951(86)90195-2

KING, R. F. 1955. The remanent magnetism of artificially deposited sediments. *Geophysical Journal International*, **7**, 115–134.

KIRSCHVINK, J. L. 1980. The least-square line and plane and the analysis of paleomagnetic data. *Geophysical*

Journal of the Royal Astronomical Society, **62**, 699–718.

KRÖNER, A. & ŞENGÖR, A. M. C. 1990. Archean and Proterozoic ancestry in late Precambrian to early Paleozoic crustal elements of southern Turkey as revealed by single-zircon dating. *Geology*, **18**, 1186–1190, http://doi.org/10.1130/0091-7613(1990)018<1186: AAPAIL>2.3.CO;2

LEFEBVRE, C., MEIJERS, M. J. M., KAYMAKCI, N., PEYNIRCIOGLU, A., LANGEREIS, C. G. & VAN HINSBERGEN, D. J. J. 2013. Reconstructing the geometry of central Anatolia during the late Cretaceous: large-scale Cenozoic rotations and deformation between the Pontides and Taurides. *Earth and Planetary Science Letters*, **366**, 83–98. http://doi.org/10.1016/j.epsl.2013.01.003

MADANIPOUR, S., EHLERS, T. A., YASSAGHI, A., REZAEIAN, M., ENKELMANN, E. & BAHROUDI, A. 2013. Synchronous deformation on orogenic plateau margins: insights from the Arabia–Eurasia collision. *Tectonophysics*, **608**, 440–451. http://doi.org/10.1016/j.tecto.2013.09.003

MCFADDEN, P. L. & MCELHINNY, L. W. 1988. The combined analysis of remagnetization circles and direct observations in palaeomagnetism. *Earth and Planetary Science Letters*, **87**, 161–172.

MCFADDEN, P. L. & MCELHINNY, M. W. 1990. Classification of the reversal test in palaeomagnetism. *Geophysical Journal International*, **103**, 725–729.

MEIJERS, M. J. M., KAYMAKCI, N., VAN HINSBERGEN, D. J. J., LANGEREIS, C. G., STEPHENSON, R. A. & HIPPOLYTE, J. C. 2010. Late Cretaceous to Paleocene oroclinal bending in the central Pontides (Turkey). *Tectonics*, **29**, TC4016. http://doi.org/10.1029/2009TC002620.

MEIJERS, M. J. M., SMITH, B. *ET AL.* 2015. A paleolatitude reconstruction of the South Armenian Block since the late Cretaceous: constraints on the Tethyan realm. *Tectonophysics*, **644–645**, 197–219. http://doi.org/10.1016/j.tecto.2015.01.012

MOSAR, J., KANGARLI, T., BOCHUD, M., GLASMACHER, U. A., RAST, A., BRUNET, M.-F. & SOSSON, M. 2010. Cenozoic-Recent tectonics and uplift in the Greater Caucasus: a perspective from Azerbaijan. *In*: SOSSON, M., KAYMAKCI, N., STEPHENSON, R. A., BERGERAT, F. & STAROSTENKO, V. (eds) *Sedimentary Basin Tectonics from the Black Sea and Caucasus to the Arabian Platform*. Geological Society, London, Special Publications, **340**, 261–280. http://doi.org/10.1144/SP340.12

MOUTHEREAU, F. 2011. Timing of uplift in the Zagros belt/Iranian plateau and accommodation of late Cenozoic Arabia–Eurasia convergence. *Geological Magazine*, **148**, 726–738. http://doi.org/10.1017/S0016756811000306

MULLENDER, T. A. T., VAN VELZEN, A. J. & DEKKERS, M. J. 1993. Continuous drift correction and separate identification of ferromagnetic and paramagnetic contributions in thermomagnetic runs. *Geophysical Journal International*, **114**, 663–672.

OKAY, A. I. 2008. Geology of Turkey: A synopsis. *Anschnitt*, **21**, 19–42.

OKAY, A. I. & ŞAHINTÜRK, Ö. 1997. Geology of the Eastern Pontides. *In*: ROBINSON, A. G. (ed.) *Regional and*

Petroleum Geology of the Black Sea and Surrounding Region. AAPG Memoir, **68**, 291–311.

OKAY, A. I., TÜYSÜZ, O., SATIR, M., ÖZKAN-ALTINER, S., ALTINER, D., SHERLOCK, S. & EREN, R. H. 2006. Cretaceous and Triassic subduction-accretion, HP/LT metamorphism and continental growth in the Central Pontides, Turkey. *Geological Society of America Bulletin*, **118**, 1247–1269.

OKAY, A. I., ZATTIN, M. & CAVAZZA, W. 2010. Apatite fission-track data for the Miocene Arabia-Eurasia collision. *Geology*, **38**, 35–38. http://doi.org/10.1130/G30234.1

ÖZDEMIR, Ö. & DUNLOP, D. J. 1996. Thermoremanence and Néel temperature of goethite. *Geophysical Research Letters*, **23**, 921–924. http://doi.org/10.1029/96GL00904

PAFFENHOLTZ, K. N. 1959. *Geological History of the Caucasus.* Izdatelstvo NAS Armenia SSR, Yerevan [in Russian].

REILINGER, R., MCCLUSKY, S. ET AL. 2006. GPS constraints on continental deformation in the Africa–Arabia–Eurasia continental collision zone and implications for the dynamics of plate interactions. *Journal of Geophysical Research*, **111**, B05411. http://doi.org/10.1029/2005JB004051

REZAEIAN, M., CARTER, A., HOVIUS, N. & ALLEN, M. B. 2012. Cenozoic exhumation history of the Alborz Mountains, Iran: new constraints from low-temperature chronometry. *Tectonics*, **31**. TC2004, http://doi.org/10.1029/2011TC002974

RICE, S. P., ROBERTSON, A. H. F. & USTAÖMER, T. 2006. Late Cretaceous–Early Cenozoic tectonic evolution of the Eurasian active margin in the Central and Eastern Pontides, northern Turkey. *In*: ROBERTSON, A. H. F. & MOUNTRAKIS, D. (eds) *Tectonic Development of the Eastern Mediterranean Region.* Geological Society, London, Special Publications, **260**, 413–445. http://doi.org/10.1144/GSL.SP.2006.260.01.17

RITZ, J. F., NAZARI, H., GHASSEMI, A., SALAMATI, R., SHAFEI, A., SOLAYMANI, S. & VERNANT, P. 2006. Active transtension inside central Alborz: a new insight into northern Iran–southern Caspian geodynamics. *Geology*, **34**, 477–480. http://doi.org/10.1130/g22319.1

ROBERTSON, A. H. F., PARLAK, O., USTAOMER, T., TASLID, K., İNAND, N., DUMITRICAE, P. & KARAOĞLAN, F. 2014. Subduction, ophiolite genesis and collision history of Tethys adjacent to the Eurasian continental margin: new evidence from the Eastern Pontides, Turkey. *Geodinamica Acta*, **26**, 230–293. http://doi.org/10.1080/09853111.2013.877240

ROBINSON, A. G., BANKS, C. J., RUTHERFORD, M. M. & HIRST, J. P. P. 1995. Stratigraphic and structural development of the Eastern Pontides, Turkey. *Journal of the Geological Society,* **152**, 861–872. http://doi.org/http://doi.org/10.1144/gsjgs.152.5.0861

ROLLAND, Y., BILLO, S., CORSINI, M., SOSSON, M. & GALOYAN, G. 2009a. Blueschists of the Amassia-Stepanavan Suture Zone (Armenia): linking Tethys subduction history from E-Turkey to W-Iran. *International Journal of Earth Sciences*, **98**, 533–550.

ROLLAND, Y., GALOYAN, G. ET AL. 2009b. Jurassic back-arc and Cretaceous hot-spot series in the Armenian ophiolites – implications for the obduction process. *Lithos*, **112**, 163–187.

ROLLAND, Y., SOSSON, M., ADAMIA, SH. & SADRADZE, N. 2011. Prolonged Variscan to Alpine history of an active Eurasian margin (Georgia, Armenia) revealed by $^{40}Ar/^{39}Ar$ dating. *Gondwana Research*, **20**, 798–815.

ROLLAND, Y., PERINCEK, D., KAYMAKCI, N., SOSSON, M., BARRIER, E. & AVAGYAN, A. 2012. Evidence for 80–75 Ma subduction jump during Anatolide–Tauride–Armenian block accretion and 48 Ma Arabia–Eurasia collision in Lesser Caucasus–East Anatolia. *Journal of Geodynamics*, **56–57**, 76–85.

SADRADZE, N. 2015. *Geodynamics of the continental collision zone on the example of post-collisional volcanism evolution in southern Georgia (Javakheti and adjacent area).* PhD thesis, Tbilisi, St. Andrew the First-Called Georgian University of the Patriarchate of Georgia [in Georgian with Abstract in English].

SAINTOT, A., STEPHENSON, R. A., STOVBA, S., BRUNET, M.-F., YEGOROVA, T. & STAROSTENKO, V. 2006. The evolution of the southern margin of eastern Europe (Eastern European and Scythian platforms) from the latest Precambrian–Early Palaeozoic to the Early Cretaceous. *In*: GEE, D. G. & STEPHENSON, R. A. (ed.) *European Lithosphere Dynamics.* The Geological Society, London, Memoirs, **32**, 481–505, http://doi.org/10.1144/GSL.MEM.2006.032.01.30

SCHWARTZ, S. Y. & VAN DER VOO, R. 1983. Paleomagnetic study of thrust sheet rotation during foreland impingement in the Wyoming-Idaho overthrust belt. *Journal of Geophysical Research*, **89**, 10077–10086. http://doi.org/10.1029/JB089iB12p10077

ŞENGÖR, A. M. C., GÖRÜR, N. & SAROĞLU, F. 1985. Strike-slip faulting and basin related formation in zones of tectonic escape: Turkey as a case study. *In*: BIDDLE, K. T. & CHRISTIE-BLICK, N. (eds) *Strike-Slip Deformation, Basin Formation, and Sedimentation.* Society of Economic Paleontologists and Mineralogists, Special Publication, **37**, 227–440.

SI, J. & VAN DER VOO, R. 2001. Too-low magnetic inclinations in central Asia: an indication of a long-term Tertiary non-dipole field? *Terra Nova*, **13**, 471–478. http://doi.org/10.1046/j.1365-3121.2001.00383.x

SOSSON, M., ROLLAND, Y. ET AL. 2010. Subduction, obduction and collision in the Lesser Caucasus (Armenia, Azerbaijan, Georgia), new insights. *In*: SOSSON, M., KAYMAKCI, N., STEPHENSON, R. A., BERGERAT, F. & STAROSTENKO, V. (eds) *Sedimentary Basin Tectonics from the Black Sea and Caucasus to the Arabian Platform.* Geological Society, London, Special Publications, **340**, 329–352. http://doi.org/10.1144/SP340.140305-8719/10

TAUXE, L. & WATSON, G. S. 1994. The fold test: an eigen analysis approach. *Earth and Planetary Science Letters*, **122**, 331–341.

TAUXE, L., KODAMA, K. P. & KENT, D. V. 2008. Testing corrections for paleomagnetic inclination error in sedimentary rocks: a comparative approach. *Physics of the Earth and Planetary Interiors*, **169**, 152–165.

TOPUZ, G., GÖÇMENGIL, G., ROLLAND, Y., ÇELIK, Ö. F., ZACK, T. & SCHMITT, A. K. 2013. Jurassic accretionary complex and ophiolite from northeast Turkey: no

evidence for the Cimmerian continent. *Geology*, **41**, 255–258.

TORSVIK, T. H., VAN DER VOO, R. *ET AL.* 2012. Phanerozoic polar wander, palaeogeography and dynamics. *Earth-Science Reviews*, **114**, 325–368.

TÜYSÜZ, O. 1999. Geology of the Cretaceous sedimentary basins of the Western Pontides. *Geological Journal*, **34**, 75–93.

TÜYSÜZ, O. & TEKIN, U. K. 2007. Timing of imbrication of an active continental margin facing the northern branch of Neotethys, Kargı Massif, northern Turkey. *Cretaceous Research*, **28**, 854–764.

TÜYSÜZ, O., DELLALOGLU, A. A. & TERZIOGLU, N. 1995. A magmatic belt within the Neo-Tethyan suture zone and its role in the tectonic evolution of northern Turkey. *Tectonophysics*, **243**, 173–191.

USTAÖMER, T. & ROBERTSON, A. H. F. 2010. Late Palaeozoic–Early Cenozoic tectonic development of the Eastern Pontides (Artvin area), Turkey: stages of closure of Tethys along the southern margin of Eurasia. *In*: SOSSON, M., KAYMAKCI, N., STEPHENSON, R. A., BERGERAT, F. & STAROSTENKO, V. (eds) *Sedimentary Basin Tectonics from the Black Sea and Caucasus to the Arabian Platform*. Geological Society, London, Special Publications, **340**, 281–327. http://doi.org/10.1144/SP340.13

VAN VELZEN, A. J. & ZIJDERVELD, J. D. A. 1995. Effects of weathering on single domain magnetite in early Pliocene marls. *Geophysical Journal International*, **121**, 267–278.

VINCENT, S. J., MORTON, A. C., CARTER, A., GIBBS, S. & BARABADZE, T. G. 2007. Oligocene uplift of the western Greater Caucasus: an effect of initial Arabia–Eurasia collision. *Terra Nova*, **19**, 160–166. http://doi.org/10.1111/j.1365-3121.2007.00731.x

VINCENT, S. J., HYDEN, F. & BRAHAM, W. 2014. Along-strike variations in the composition of sandstones derived from the uplifting western Greater Caucasus:

causes and implications for reservoir quality prediction in the Eastern Black Sea. *In*: SCOTT, R. A., SMYTH, H. R., MORTON, A. C. & RICHARDSON, N. (eds) *Sediment Provenance Studies in Hydrocarbon Exploration and Production*. Geological Society, London, Special Publications, **386**, 111–127. http://doi.org/10.1144/SP386.15

WATSON, G. 1983. Large sample theory of the Langevin distributions. *Journal of Statistical Planning and Inference*, **8**, 245–256.

WEIL, A. B. & SUSSMAN, A. J. 2004. Classifying curved orogens based on timing relationships between structural development and vertical-axis rotations. *In*: SUSSMAN, A. J. & WEIL, A. B. (eds) *Orogenic Curvature: Integrating Paleomagnetic and Structural Analyses*. Geological Society of America, Special Papers, **383**, 1–15.

YILMAZ, C. & KANDEMIR, R. 2006. Sedimentary records of the extensional tectonic regime with temporal cessation: Gumushane Mesozoic Basin (NE Turkey). *Geologica Carpathica*, **57**, 3–13.

YILMAZ, A., ADAMIA, SH., CHABUKIANI, A., CHKHOTUA, T., ERDOĞAN, K., TUZCU, S. & KARABIYIKOĞLU, M. 2000. Structural correlation of the southern Transcaucasus (Georgia)-eastern Pontides (Turkey). *In*: BOZKURT, E., WINCHESTER, J. A. & PIPER, J. D. A. (eds) *Tectonics and Magmatism in Turkey and the Surrounding Area*. Geological Society, London, Special Publications, **173**, 171–182. http://doi.org/10.1144/GSL.SP.2000.173.01.08

YONKEE, A. & WEIL, A. B. 2010. Quantifying vertical axis rotation in curved orogens: correlating multiple data sets with a refined weighted least squares strike test. *Tectonics*, **29**, 31.

ZIJDERVELD, J. D. A. 1967. A.C. demagnetization of rocks: analysis of results. *In*: COLLINSON, D. W., CREER, K. M. & RUNCORN, S. K. (eds) *Methods in Palaeomagnetism*. Elsevier, Amsterdam, 254–286.